

Monitoring desertification in Mongolia based on Landsat images and Google Earth Engine from 1990 to 2020



Xiaoyu Meng^{a,b}, Xin Gao^{a,b,*}, Sen Li^c, Shengyu Li^{a,b}, Jiaqiang Lei^{a,b}

^a State Key Laboratory of Desert and Oasis Ecology, Xinjiang Institute of Ecology and Geography, Chinese Academy of Sciences, 818 South Beijing Road, Urumqi 830011, Xinjiang, China

^b University of Chinese Academy of Sciences, Beijing 100049, China

^c Key Laboratory of Desert and Desertification, Northwest Institute of Eco-Environment and Resources, Chinese Academy of Sciences, 260 West Donggang Road, Lanzhou 730000, Gansu, China

ARTICLE INFO

Keywords:

GEE
Machine learning methods
Desertification dynamics
Gravity center change
Intensity analysis
Desertification maps
Mongolia

ABSTRACT

Desertification is one of the most serious ecological and environmental problems in arid regions. Low-cost, wide-ranging, and high-precision methods are essential for the formulation of appropriate strategies for quantitatively monitoring desertification. In this study, based on Google Earth Engine and Landsat images, six machine learning methods were used to monitor desertification dynamics in 1990–2020 in Mongolia. The spatiotemporal distributions and changes in desertification at different stages were analyzed using gravity center change and intensity analysis models. Subsequently, we quantitatively investigated the factors driving desertification in Mongolia. The results indicate that the maximum entropy method can obtain the most accurate assessment of the degree of desertification in comparison with the other five methods, with an accuracy of 96%. In 1990–2005, the area of desertified land increased significantly; afterward, a decreasing trend was observed. Lightly and moderately desertified lands had the highest change intensities and were most sensitive to environmental factors. Although the desertification dynamics are under the influence of both natural and anthropogenic factors, precipitation plays a dominant role in Mongolia. This study provides a comprehensive analysis of the desertification status and trends in Mongolia, and presents desertification maps that can be used to formulate preventive measures and guide desertification prevention and control.

1. Introduction

Desertification is one of the most serious global ecological and environmental problems, and it affects 1/5 of the world's population, which lives in arid lands (Ma and Zhao, 1994). Mongolia is a hotspot of global desertification (Eckert et al., 2015). Approximately 90% of Mongolia is at risk of desertification, with 41.3% considered deserts and desert steppe areas (Dorj et al., 2013). Desertification also has a significant impact on the Mongolia's animal husbandry, directly affecting the country's economy and residents' living standards. In addition, intensification of desertification has increased wind erosion and dust emission sources, which threatens the air quality in leeward countries in East Asia (Jugder et al., 2011; Kimura and Shinoda, 2010). Clarifying the distribution and extent of desertification is a basis for the formulation of appropriate desertification control policies. However, no

national, long-term, high-spatial-resolution desertification dataset exists in Mongolia which hinders the formulation and implementation of desertification control measures. Hence, it is necessary to establish a complete desertification information extraction process based on remote sensing technologies to rapidly and accurately assess the status of desertification and reveal the causes of desertification development.

Desertification monitoring methods include field survey monitoring, remote sensing image classification monitoring, and desertification indicator monitoring (Zhang and Huisingsh, 2018). In comparison with conventional field survey monitoring, remote sensing and image classification technologies are rapid methods of extracting desertification information. The methods can be categorized into human-computer interactive visual interpretation methods and automatic classification methods (i.e., supervised and unsupervised classification) (Zhang et al., 2018a). Visual interpretation has the advantage of high accuracy (Duan

* Corresponding author at: State Key Laboratory of Desert and Oasis Ecology, Xinjiang Institute of Ecology and Geography, Chinese Academy of Sciences, 818 South Beijing Road, Urumqi 830011, Xinjiang, China.

E-mail address: gaoxin@ms.xjb.ac.cn (X. Gao).

et al., 2019). However, because of the time-consuming process and the influence of human factors, it is difficult to monitor desertification on a large scale over the long term (Duan et al., 2019). Conversely, automatic classification methods require relatively short periods and are suitable for monitoring large areas of desertification (Na et al., 2019). Unsupervised classification methods use clustering methods (e.g., K-means) to classify images, and human expertise is not required in such processes (Wu et al., 2019). Generally, unsupervised methods are rapid and have low labor costs; however, the accuracy of the classification results depends on the quality and distribution of data (Wu et al., 2019). Supervised classification methods involve the training of classification models based on manually selected sampling points and extensions to other pixels over entire study areas. Owing to the artificial auxiliary training, the classification results are more accurate (Duan et al., 2019; Xu et al., 2019; Liu et al., 2018). Monitoring methods based on desertification indicators mainly include the single indicator method and multiple indicator method. When using a single indicator to evaluate desertification, most studies used vegetation index thresholds to classify the degree of desertification (Bezerra et al., 2020; Filei et al., 2018). Evidently, this method only considers vegetation cover and ignores soil information, leading to the lower accuracy of the classification results (Wei et al., 2018). The multiple indicator method includes two categories: use of the feature space models for classification, and use of machine learning methods to construct evaluation models and classification criteria. Common feature space models include the albedo-normalized differential vegetation index (NDVI) model (Wei et al., 2020) and point-point model (Guo et al., 2020). Because such models only consider two indicators, it is difficult to accurately monitor complex desertification information (Duan et al., 2019). In the common multiple indicator classification methods based on machine learning methods, the indicators mainly include the NDVI, albedo, topsoil grain size index (TGSI), and land surface temperature (Guo et al., 2020; Wei et al., 2020, 2018; Duan et al., 2019). Common machine learning methods include decision trees and the random forest (RF) method (Duan et al., 2019; Lamchin et al., 2016). However, at present, the performance of other machine learning methods in desertification monitoring remains unclear. To improve the technologies and methods of desertification mapping, it is necessary to comprehensively evaluate the performance of multiple machine learning methods in desertification research.

In the wake of advancements in cloud computing technologies, Google launched the Google Earth Engine (GEE) cloud computing platform in 2010. GEE can be used for planet-star geospatial data analyses and provides significant image data support (Gorelick et al., 2017). In comparison with traditional image processing tools, GEE can rapidly batch process image data, thereby reducing the cost and complexity of geospatial data analysis. It has been used as the main computing platform for numerous scientific earth system studies, including land-use and land-cover change detection (Huang et al., 2017; Midekisa et al., 2017; Hansen et al., 2013), crop mapping (Teluguntla et al., 2018; Shelestov et al., 2017), and wetland mapping (Wu et al., 2019; Hird et al., 2017). The emergence of the GEE platform had enabled rapid monitoring and mapping of desertification over large scales and over the long term.

In the case of desertification in Mongolia, some issues remain unresolved, which hamper the formulation of appropriate policies to combat desertification, as follows. (1) In Mongolia, there are largely low-spatial-resolution desertification datasets. The coarse resolution pixels often contain different land cover types (i.e., mixed pixels), which often impede the development and implementation of appropriate desertification control measures in local areas (Lamchin et al., 2016). In addition, (2) the majority of existing studies on desertification monitoring in Mongolia have focused on local settings (Wei et al., 2020, 2018; Lamchin et al., 2016) and short-term monitoring (Lee et al., 2019; Lin et al., 2006). The scattered research cannot provide comprehensive information on desertification in Mongolia at the national level. Furthermore, (3) many factors influence desertification, including climate change and

human activities (Lanckriet et al., 2016; Spinoni et al., 2015). Under complex climate change and human activities, desertification development trends in different regions of Mongolia demonstrate different patterns (Wei et al., 2020, 2018; Sanzheev et al., 2020), proving that the relative importance of factors is an important basis for desertification control. Previous studies on the key factors driving desertification in Mongolia have been largely limited to single or a few factors (Wang et al., 2017; Zolotokrylin et al., 2016; Garchinbyamba and Kang, 2013), which makes it challenging to comprehensively evaluate the role of environmental factors in promoting desertification.

This study aimed to monitor desertification in Mongolia based on the GEE platform using Landsat image data. We analyzed the spatiotemporal characteristics of desertification in Mongolia in 1990–2020 and revealed its driving forces. Based on all Landsat images in 1990–2020 in Mongolia, extensive ground surveys, and the existing desertification classification system, we used decision tree, support vector machine (SVM), RF, naive Bayes (NB), minimum distance (MD), and maximum entropy (ME) classifiers, to extract desertification information for seven periods (1990, 1995, 2000, 2005, 2010, 2015, and 2020). Finally, according to the most accurate classification method, we constructed a 30-m desertification map for the seven periods. The specific objectives of the present study were to: (1) monitor desertification development in Mongolia using GEE; (2) clarify the temporal and spatial distribution and changes in desertification in Mongolia; and (3) reveal the factors driving desertification changes in Mongolia from 1990 to 2020.

2. Materials and methods

2.1. Study area

Mongolia is a landlocked country in East Asia; it borders Russia to the north and China to the south, and is located between 41.5 and 52.1°N and 87.70–119.9°E (Fig. 1). The northern and western parts of Mongolia are mountainous areas with considerable changes in elevation, and the Gobi Desert in the south is relatively flat with a mean elevation of 1,058 m (Meng et al., 2020). Mongolia's unique geographical location results in obvious continental climate characteristics, including intensely cold winters and hot summers, and large annual and daily temperature differences. From south to north, Mongolia's vegetation types are the Gobi Desert, steppes, and forests. Forests are concentrated roughly parallel to the latitude, in the mountains in the north and west. Steppes are mainly distributed in the central and eastern parts of Mongolia. The Gobi Desert is mainly distributed in the southwest, where vegetation is sparse and rare. Mongolia's forest and steppe areas account for 7% and 42% of the total area of the country, respectively (Wang et al., 2019). According to statistics from the National Statistics Office of Mongolia, Mongolia has a total population of 3,296,866 and a land area of $1.56 \times 10^4 \text{ km}^2$, indicating that Mongolia has a low population density. A total of 250,000 people are engaged in animal husbandry in Mongolia, and most herders operate in a nomadic or semi-nomadic manner.

2.2. Data

This study monitored desertification in Mongolia and analyzed the spatial and temporal characteristics of desertification and its driving forces using preprocessed Landsat image data. Fig. 2 is a flowchart of our research, which can be divided into four parts: (1) data preprocessing and the extraction of desertification indicators; (2) desertification mapping; (3) analysis of temporal and spatial changes; and (4) driving force analysis.

2.2.1. Landsat images

The present study mapped desertification distributions in 1990, 1995, 2000, 2005, 2010, 2015, and 2020 in Mongolia. To produce high-quality pixel composites for each period, we used a three-year synthesis method to minimize atmospheric noise and interannual phenological

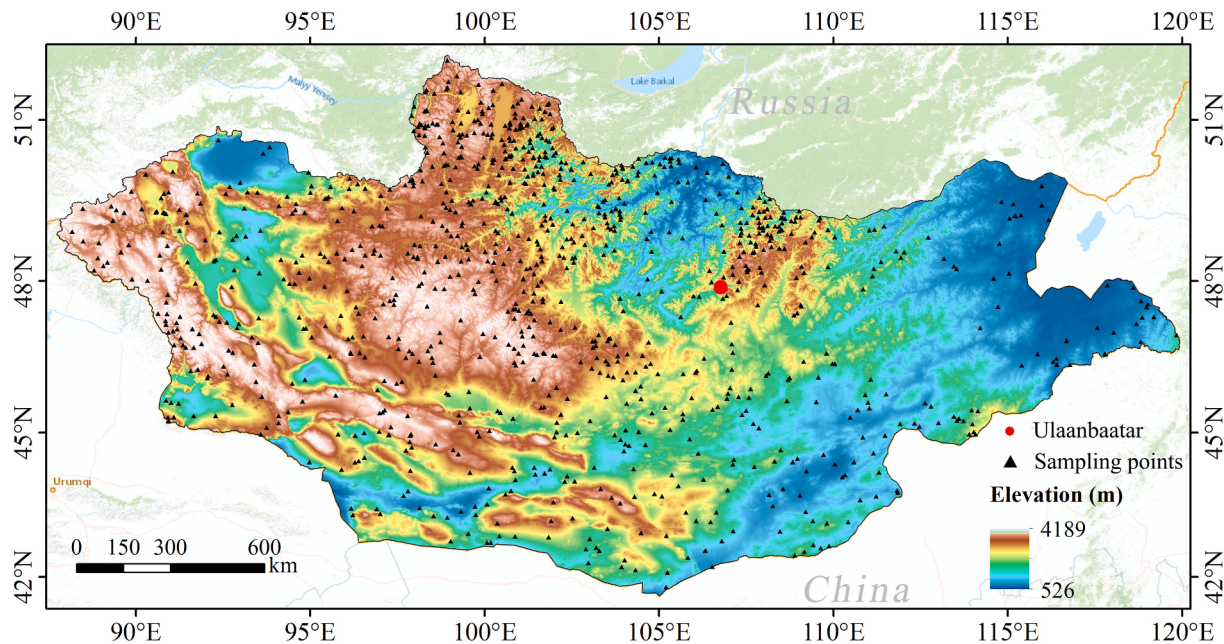


Fig. 1. Geographical features of Mongolia and the sampling points for machine learning methods. The elevation data is from the Shuttle Radar Topography Mission (SRTM) dataset (<https://srtm.csi.cgiar.org/>).

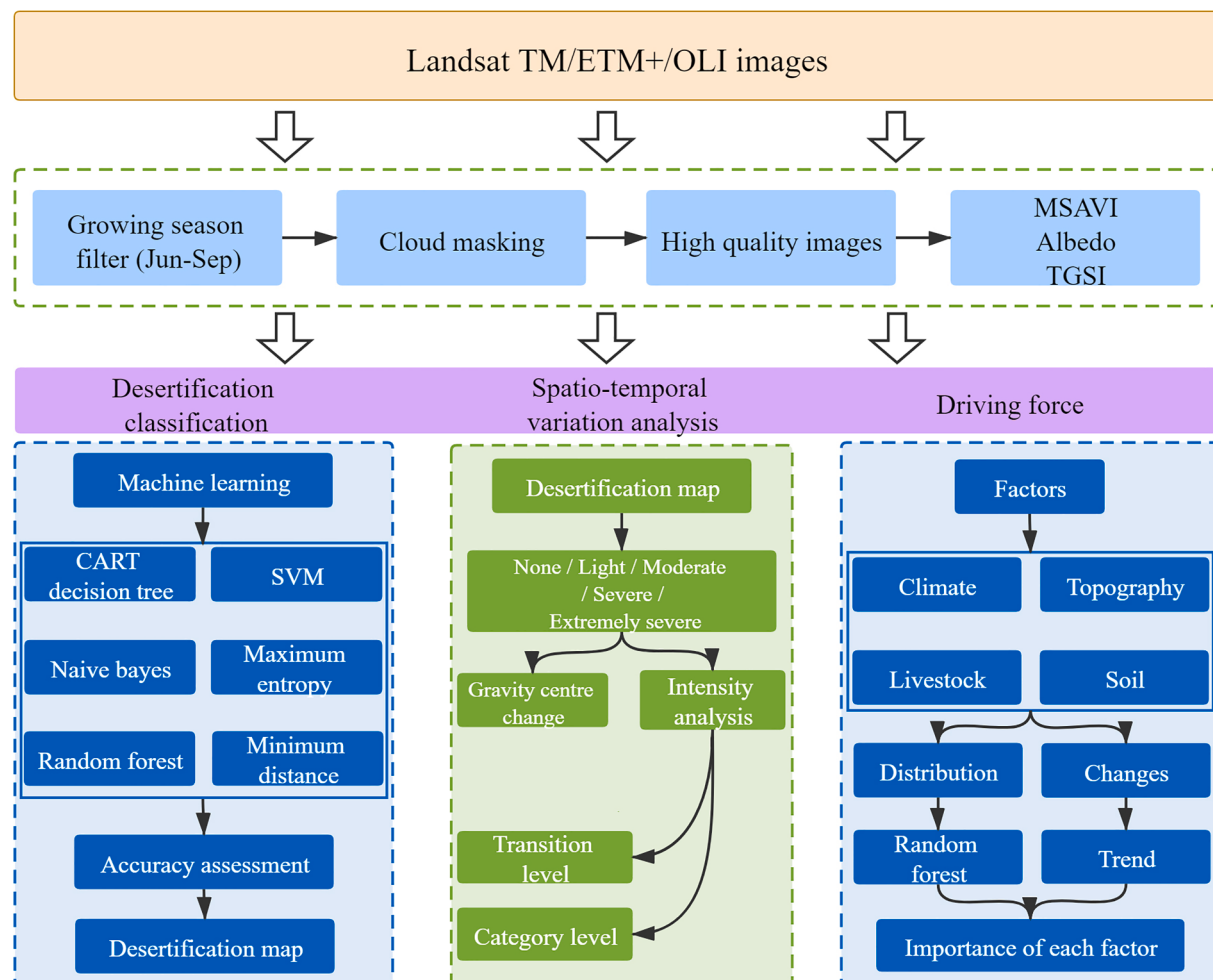


Fig. 2. Methodological flowchart for this study.

variations (Chen et al., 2020). For example, the image data of 1990 were stitched using good-quality pixels of images in 1989, 1990, and 1991. Data for 2020 were a synthesis of the growing-season images of 2019 and 2020. The number of Landsat 5, 7, and 8 surface reflectance images within the study period are depicted in Fig. 3a. The distributions of good-quality observations for each Landsat pixel location at each time node are illustrated in Fig. 3b. The results showed that there were 10 good-quality observations for most pixels in 1990 and 1995, 30–40 effective observations for most pixels in 2000, 2005, 2010, and 2015, and approximately 20 effective observations in 2020. The number of observations of some pixels in 1990 was 0 (the minimum value of the violin figure in 1990 is 0 in Fig. 3b). Such unobserved pixels were located in the mountainous areas of western Mongolia, and the land-cover type is a glacier with an area of approximately 31 km². Considering that the unobserved area is small and the land-cover type is glacier land, we assumed that it has little influence on the subject of the present study.

There was at least one high-quality observation for each pixel during the study period. Here, we selected Landsat surface reflectance Tier 1, which has completed atmospheric and geometric corrections as well as cross-calibration between different sensors (Dwyer et al., 2018; Wulder et al., 2016), for analyzing long-term changes in desertification. For each image, the cloud, cloud shadow, and snow pixels were removed using the data quality layer from the CFmask cloud masking method (Zhou et al., 2019; Zhu and Woodcock, 2014; Zou et al., 2018). To date, seven phases of high-quality growing season Landsat image collections of Mongolia with a 30 × 30-m resolution have been prepared.

2.2.2. Meteorological factors

Meteorological factors, such as precipitation, vapor pressure deficit (VPD), potential evapotranspiration (PE), and wind speed are important factors that affect the development of desertification (Wei et al., 2020; Zhu et al., 2020; Jiang et al., 2019; Wang et al., 2019). Atmospheric VPD is a vital factor in determining plant photosynthesis (Yuan et al., 2019). Leaf and canopy photosynthetic rates decline when VPD increases due to stomatal closure (Zhang et al., 2018b). These four meteorological factors were used to assess the driving force for the distribution and change in desertification in Mongolia, which were acquired from TerraClimate data (Abatzoglou et al., 2018). TerraClimate is a dataset of monthly climate and climatic water balance for global terrestrial surfaces in

1958–2019 with a ~ 4-km (1/24th degree) spatial resolution. In this study, we calculated the annual mean values of each meteorological factor for each period corresponding to Landsat data (Fig. 4a–d).

2.2.3. Topographical factors

Topographical factors indirectly influence vegetation distribution and growth (Meng et al., 2020). In the present study, we selected elevation, slope degree, and slope aspect as the topographical factors affecting the development of desertification. The factors were directly derived from the digital elevation model (DEM). The DEM dataset used in the present study was the Shuttle Radar Topography Mission digital elevation data (Fig. 4e–g).

2.2.4. Livestock

The occurrence and development of desertification are inevitably affected by grazing activity, which is also one of the major factors considered to aggravate desertification in arid regions (Jiang et al., 2019; Zolotokrylin et al., 2016). We obtained the number of livestock in each city between 1990 and 2015 from the National Statistics Office of Mongolia (www.1212.mn/). Through sorting and mapping, we prepared distribution maps based on annual mean number of livestock at different locations in Mongolia (Fig. 4h).

2.2.5. Soil type

Soil types influence occurrence and development of desertification to a certain extent (Jiang et al., 2019). In the present study, soil types were obtained from the book of Soil of the People's Republic of Mongolia (Bespalov, 1964). After scanning, geometrical correction, and digitization using GIS software, a map of a total of 16 soil types in Mongolia was obtained: (1) boggy soil, (2) pine sandy soil, (3) sandy soil, (4) meadow soil and boggy soil, (5) cracked alkaline soil, (6) alkali soil, (7) alkali and saline soil, (8) saline soil, (9) Gobi brown soil, (10) thin brown soil, (11) chestnut soil, (12) chestnut soil, (13) dark chestnut soil, (14) gray forest soil, (15) mountain peat soil, and (16) mountain meadow soil (Fig. 4i).

2.3. Methods

2.3.1. Desertification indicators

Vegetation amount is a key index used to characterize the degree of desertification. Vegetation index is often used to represent vegetation

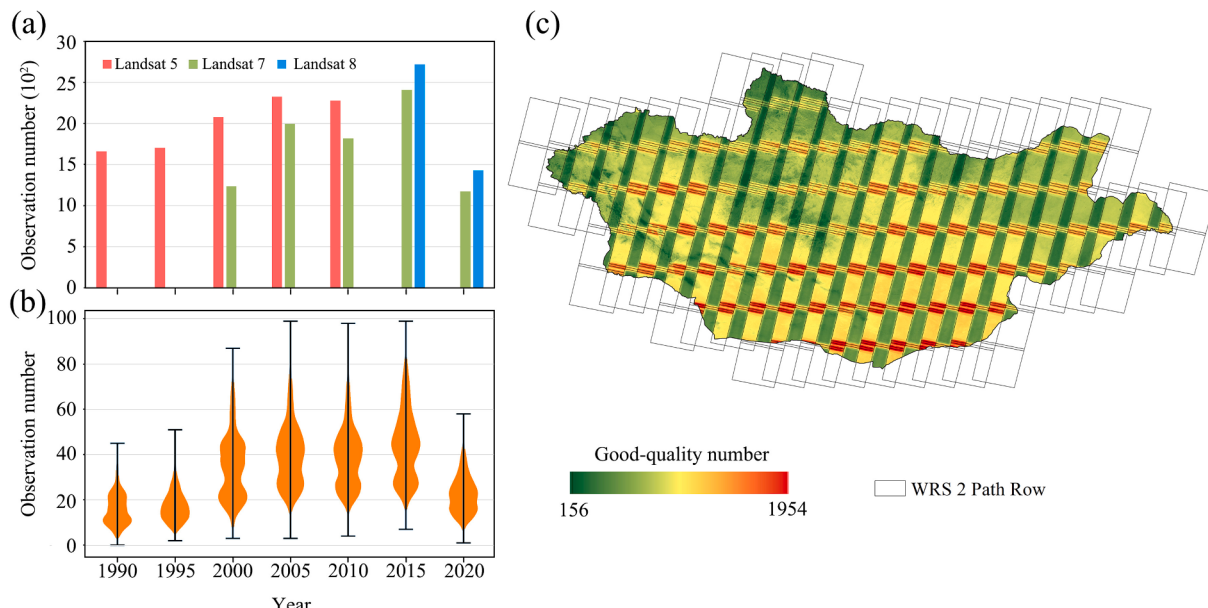


Fig. 3. Statistics of Landsat observations across Mongolia. (a) Total observation number of different Landsat satellites. (b) Observation number of the pixels of each period. (c) Spatial distributions of good-quality Landsat observations.

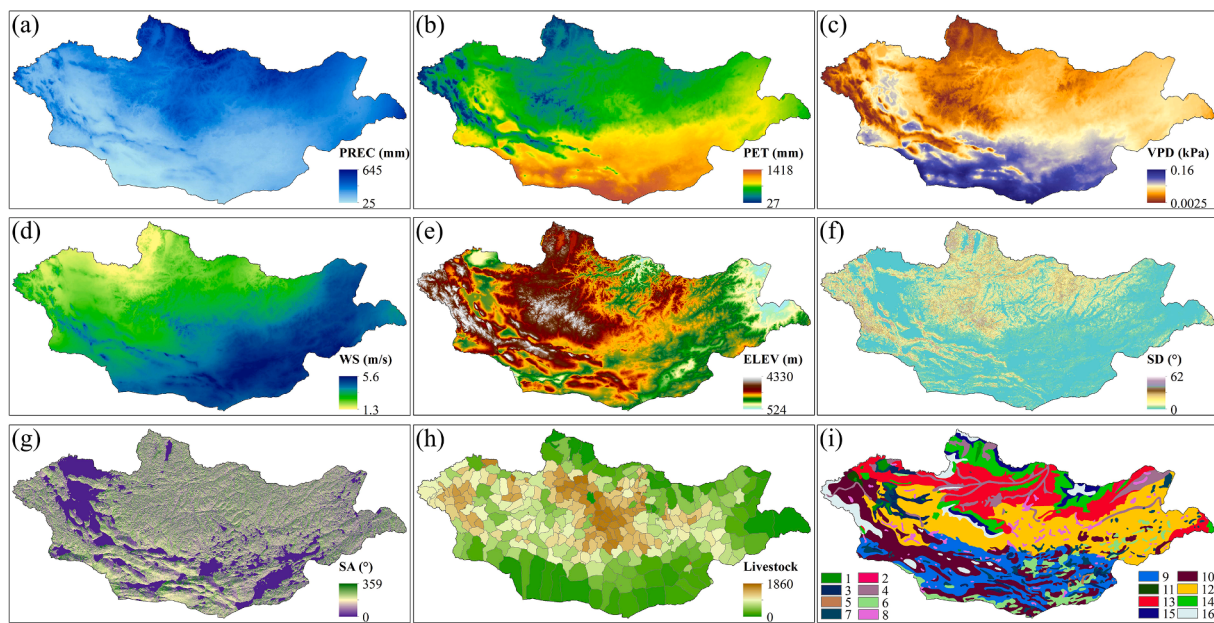


Fig. 4. Spatial distributions of environmental factors. (a) Precipitation (PREC), (b) potential evapotranspiration (PET), (c) vapor pressure deficit (VPD), (d) wind speed (WS), (e) elevation (ELEV), (f) slope degree (SD), (g) slope aspect (SA), (h) number of livestock (LIVESTOCK), and (i) soil type (SOIL).

growth status, and the commonly used vegetation index is NDVI. However, owing to the influence of soil background on NDVI, vegetation growth status cannot be adequately represented in areas with sparse vegetation (Guo et al., 2020; Wei et al., 2020). Therefore, Qi et al. (1994) proposed a modified soil adjusted vegetation index (MSAVI), which fully considers the soil background and can better exclude the influence of soil. MSAVI is often used to assess vegetation status in arid areas (Wei et al., 2020; Duan et al., 2019), and is calculated using the following equation:

$$\text{MSAVI} = \left(2\text{NIR} + 1 - \sqrt{(2\text{NIR} + 1)^2 - 8(\text{NIR}-\text{RED})} \right) / 2 \quad (1)$$

where *NIR* and *RED* represent the reflectance of the near-infrared and red bands in the Landsat images, respectively.

Surface albedo refers to the ability of the Earth's surface to reflect solar radiation. It is the ratio of the solar radiation emitted by the land surface to the solar radiation energy reaching the surface (Verstraete, 1989). High ground surface albedo implies low soil quality (Robinove et al., 1981), which is a result of a decrease in soil organic matter and moisture (Rasmussen et al., 2001). Therefore, albedo can be used as an indicator in desertification monitoring activities. The equation used to calculate albedo is as follows (Liang, 2001):

$$\text{Albedo} = 0.356\text{BLUE} + 0.13\text{RED} + 0.373\text{NIR} + 0.085\text{SWIR1} + 0.072\text{SWIR2} - 0.0018 \quad (2)$$

where, *BLUE*, *RED*, *NIR*, *SWIR1*, and *SWIR2* refer to the blue band, red band, near-infrared band, first shortwave infrared band, and second shortwave infrared band in the Landsat images, respectively.

Soil texture can characterize the degree of desertification. For example, severe desertification corresponds to rough surface soil particles. Therefore, TGSi is often used an evaluation indicator for desertification (Liu et al., 2018; Wei et al., 2018). TGSi can be expressed by the following equation:

$$\text{TGSi} = (\text{RED}-\text{BLUE}) / (\text{RED} + \text{BLUE} + \text{GREEN}) \quad (3)$$

where *RED*, *BLUE*, and *GREEN* refer to the red, blue, and green bands in the Landsat images, respectively.

2.3.2. Related methods of desertification classification

To ensure the typicality and uniformity in space of the selected sampling points, we first masked the water bodies and urban construction land, which are not desertified land types (note: the water body data used in this study were obtained from the Joint Research Centre's Global Surface Water Dataset (Pekel et al., 2016). An artificial impervious surface was used to represent urban construction land (Li et al., 2020b)). Second, we used the K-means method to classify the MSAVI across the whole of Mongolia into five classes. Finally, 200 points were randomly generated within each class of the MSAVI. The selection of training sample points adheres to the stratified random sampling rule. Considering that the degree of desertification is significantly correlated with vegetation index, we classify MSAVI and randomly sample all MSAVI strata. The distribution of the 1000 sampling points is illustrated in Fig. 1.

We formulated the Mongolian desertification classification system in the present study according to the classification standards of existing studies (Duan et al., 2019; Jiang et al., 2019; Na et al., 2019; Han et al., 2010). Desertified land was classified into five levels: no, light, moderate, severe, and extremely severe desertification (Fig. 5a-d). We conducted field surveys in June-September (i.e., the vegetation growing season in Mongolia) in 2019 and 2020, during which we used 1 × 1 m and 10 × 10 m quadrat sampling surveys to determine vegetation cover (Fig. 5e and f). Combined with the Google Earth high-resolution images during the same period, we labeled the 1000 sampling points with five desertification levels. The characteristics of the desertified landscapes for each level of desertification are listed in Table 1. In GEE, we randomly split the sampling points into 70% and 30% ratios as training samples and validation samples, respectively. In the machine learning classifier training process, we randomly run each method five times to ensure that the classifier performance is not affected by the sampling point partitioning.

Six supervised classifiers were selected to map the desertification throughout Mongolia based on the GEE platform (Gorelick et al., 2017): Classification and regression tree (CART) (Shelestov et al., 2017; Friedl et al., 2002), Support Vector Machine (SVM) (Arabameri et al., 2020; Joshi et al., 2019; Li et al., 2020a; Vapnik, 2000), Random Forest (RF) (Belgiu and Drăguț, 2016; Chan and Paelinckx, 2008; Breiman, 2001), Naive Bayes (NB) (Arabameri et al., 2020; Miranda et al., 2020; Tang et al., 2020; Gustafsson et al., 2010), Maximum Entropy (ME) (Elith

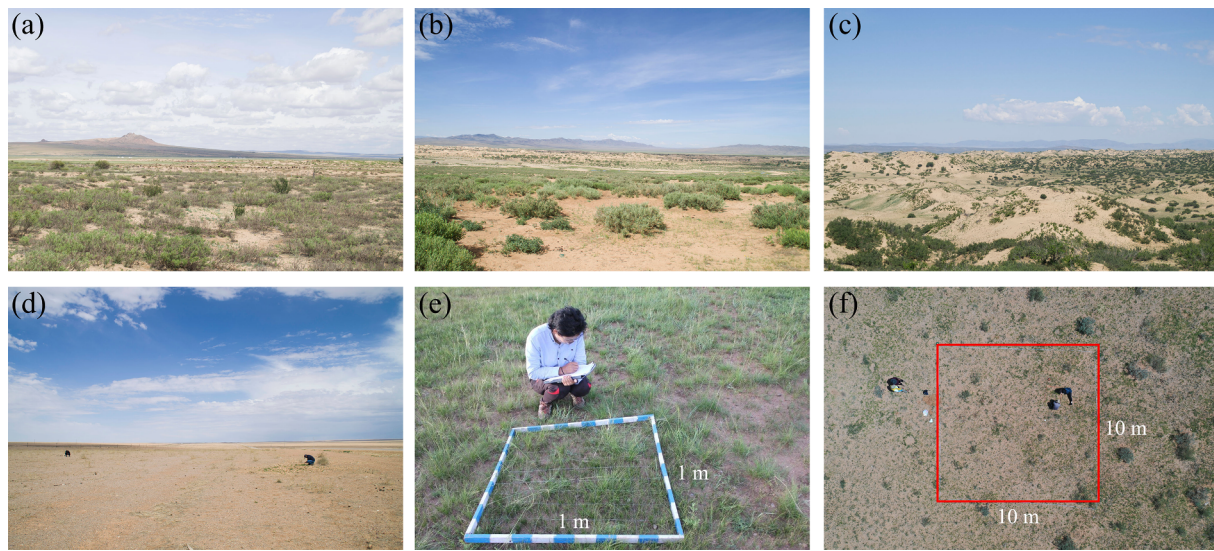


Fig. 5. Landscape photographs of desertification in Mongolia and field validation. (a) Light; (b) moderate; (c) severe; (d) extremely severe; (e) vegetation cover survey using $1\text{ m} \times 1\text{ m}$ quadrat in the lightly desertified land; (f) vegetation cover survey using $10\text{ m} \times 10\text{ m}$ quadrat in the severely desertified land obtained from a drone.

Table 1
Landscape characteristics of desertification in Mongolia.

Level	Landscape description	Vegetation cover (%)
Light	Local vegetation is degraded, and patchy sandy areas appear (5–25%)	50–70
Moderate	Vegetation is scattered, and degraded land accounts for 25–50%	10–50
Severe	The degraded area exceeds 50%. Vegetation is sparse	1–10
Extremely severe	Vegetation cover is < 10%. Mobile sandy soil is widely distributed	< 1

et al., 2011; Phillips et al., 2009; Shannon, 1948), and Minimum Distance (MD) (Lu et al., 2004).

To comprehensively evaluate the performance of each machine learning method in desertification monitoring, we used the confusion matrix and Kappa coefficient as model accuracy evaluation methods. The confusion (error) matrix is used to create a cross list of the model output class label and ground truth label of each pixel (Tang et al., 2020; Belgiu and Drăguț, 2016). The diagonal of the list is the number of pixels that are correctly classified (Foody, 2002; Congalton, 1991). The Kappa coefficient reflects the difference between the predicted class and the ground truth class, and ranges from -1 to $+1$; the larger the Kappa value, the higher the consistency between the two classification data and the better the classification method are (Bofana et al., 2020; Congalton et al., 2008; Banko, 1998).

2.3.3. Gravity center change model and intensity analysis

The gravity center change model is proposed in the context of the theory of the center of gravity of population distribution, and is used to characterize the spatial location and change in the population's center of gravity (Na et al., 2019; Jy et al., 2006). This study used the gravity center change model to calculate the distribution of different degrees of desertification, and to analyze the change in distance and direction of the gravity center to describe the spatiotemporal trends of desertification in Mongolia from 1990 to 2020. The equations for the gravity center change model are as follows:

$$X_k = \frac{\sum_{i=1}^n X_i W_{ij}}{\sum_{i=1}^n W_{ij}} \quad (4)$$

$$Y_k = \frac{\sum_{i=1}^n Y_i W_{ij}}{\sum_{i=1}^n W_{ij}} \quad (5)$$

where X_k and Y_k refer to the coordinates of the latitude and longitude of the gravity center of the k th desertification level, respectively; X_i and Y_i are the coordinates of the latitude and longitude of the gravity center of the i th pixel, respectively; and W_{ij} is the area of the j th desertification type in the i th pixel.

Intensity analysis is a relatively new method for quantitatively characterizing land-type change patterns (Na et al., 2019). In comparison with the transfer matrix, it can effectively extract important information regarding land change characteristics and processes at multiple time points (Aldwaik and Pontius, 2012). The category level and transition level are the two key levels in intensity analysis model.

The category level measures the size and intensity of the loss and gain of each type of desertification in the study area during different periods. Similarly, the intensity of a single time interval is compared with the uniform annual change intensity. If the intensity is evenly distributed throughout the study period, we consider that the change can represent the real change intensity:

$$G_{tj} = \frac{[(\sum_{i=1}^J C_{tij}) - C_{tij}]/(Y_{t+1} - Y_t)}{\sum_{i=1}^J C_{tij}} \times 100\% \quad (8)$$

$$L_{ti} = \frac{[(\sum_{j=1}^J C_{tij}) - C_{tij}]/(Y_{t+1} - Y_t)}{\sum_{j=1}^J C_{tij}} \times 100\% \quad (9)$$

where G_{tj} is the annual intensity of the gross gain of type j for time interval $[Y_t, Y_{t+1}]$ and L_{ti} is the annual intensity of the gross loss of type i for time interval $[Y_t, Y_{t+1}]$.

The transition level is intended to quantitatively describe which desertification type is particularly intensive in a time interval, and determine the intensity of any given transition from one type to another. Finally, by comparing the observed transition intensity of each type with the unified intensity, it can be determined whether the excessive intensity of each type is significant.

$$R_{tin} = \frac{C_{tin}/(Y_{t+1} - Y_t)}{\sum_{j=1}^J C_{tij}} \times 100\% \quad (10)$$

$$W_m = \frac{[(\sum_{i=1}^J C_{in}) - C_{mn}]/(Y_{t+1} - Y_t)}{\sum_{j=1}^J [(\sum_{i=1}^J C_{ij}) - C_{mj}]} \times 100\% \quad (11)$$

Here, R_{tin} is the annual intensity of transition from type i to type n during time interval $[Y_t, Y_{t+1}]$, and W_m is the value of the uniform intensity of transition to type n from all non- n types at time Y_t during time interval $[Y_t, Y_{t+1}]$.

$$Q_{tmj} = \frac{[C_{mj}/(Y_{t+1} - Y_t)]}{\sum_{i=1}^J C_{ij}} \times 100\% \quad (12)$$

$$V_{tm} = \frac{[(\sum_{j=1}^J C_{mj}) - C_{mm}]/(Y_{t+1} - Y_t)}{\sum_{i=1}^J [(\sum_{j=1}^J C_{ij}) - C_{im}]} \times 100\% \quad (13)$$

Here, Q_{tmj} is the annual intensity of transition from type m to type j during the time interval $[Y_t, Y_{t+1}]$; V_{tm} is the value of the uniform intensity of transition from type m to all non- m types at time Y_{t+1} during the time interval $[Y_t, Y_{t+1}]$; and m and n refer to the index for the losing and gaining types in the transition of interest, respectively.

2.3.4. Evaluation method of desertification driving force

The RF method estimates the importance of the independent variable by observing the extent of increase in the prediction error when the ‘out-of-bag’ data of the variable are arranged while all other data remain unchanged (Liaw and Wiener, 2002; Breiman, 2001). The importance of the factor x_j is determined as follows:

$$Importance_j = \frac{1}{N} \sum_{v \in S} G(x_j, v) \quad (14)$$

where S is the node set used to split x_j data, v is the node of S ; $G(x_j, v)$ is the RF gain of x_j , and N is the total number of trees. Thus, this gain is measured according to the impurities at each node. Some impurity criteria are used to segment the data and, therefore, quantify the importance of the features (Izquierdo-Verdiguier and Zurita-Milla, 2020; Gregorutti et al., 2017). In this study, we used this method to evaluate the importance of each environmental factor in the spatial distribution of the degrees of desertification in Mongolia.

3. Results

3.1. Classification accuracy of different machine learning methods

The validation accuracies of the CART, NB, SVM, RF, ME, and MD methods were 0.9, 0.89, 0.94, 0.9, 0.96, and 0.78, respectively, and the Kappa coefficients were 0.87, 0.85, 0.91, 0.87, 0.94, and 0.7, respectively; evidently, the classification results obtained by the ME classification method had the highest accuracy. According to the confusion matrix of the six classification methods, the CART method had a large classification error between non-desertification and light desertification (the error rate between the two levels [E] = the number of errors of the two levels/the total number of the two levels = $7/143 = 4.8\%$), and between moderate and severe desertification ($E = 12.6\%$). The main error of the NB method appeared in the process of classifying between non-desertification and light desertification ($E = 6.2\%$), and between severe and extremely severe desertification ($E = 11.9\%$). The main errors of SVM were observed for non-desertification and light desertification ($E = 5.1\%$), while the accuracies of the other levels were higher. The main errors of the RF classification method were observed for severe and moderate desertification ($E = 14.2\%$). The error classification of the ME method was not concentrated, and the number of errors was relatively small overall. The MD method exhibited the lowest accuracy, and the number of misclassifications between the two adjacent levels was relatively high. Overall, the CART, NB, SVM, RF, and ME methods performed better than the MD method in the classification of desertification. The ME, RF, and CART methods had the least numbers of

misclassifications between two non-adjacent levels (i.e., only one sample point). Therefore, we used the ME method to classify desertification in this study.

3.2. Spatiotemporal distribution of desertification in Mongolia

3.2.1. Desertification patterns during different time periods

Fig. 6 depicts the spatial distributions of different levels of desertification during different periods. Extremely severe desertification was mainly distributed in the Gobi area of southern Mongolia, and severe desertification was mainly distributed in the southeast. Moderate desertification was mainly distributed in the central and western parts, and light desertification was mainly distributed in the eastern part of Mongolia. None of the desertified lands were located in the northern and central mountainous areas. From the desertified distribution maps for different periods, the area of lightly desertified land in the east of the country increased rapidly, particularly in 1990–2000, during which the non-desertified land was mainly converted into desertified land. The moderately desertified land also expanded with the northward movement of the lightly desertified land, particularly during 1990–2000 and 2015–2020. The extensive area of lightly desertified land in eastern Mongolia transformed to moderately desertified land. From 1990 to 2020, changes between severe and extremely severe desertification have not been evident, and the majority of changes have been mutual transformations between their two types.

Fig. 7 depicts the changes in the spatial gravity center of each desertification type. The gravity center of the non-desertified and the lightly desertified land migrated from southeast to northwest, which is consistent with the results depicted in **Fig. 6**. The non-desertified land in the northeast is shrinking to the northwest, and the lightly desertified land is expanding. The gravity center of the moderately desertified land mainly migrates to the northeast and southwest, and the maximum migration distance is approximately 75 km in the longitudinal direction. The moderately desertified land is constantly transforming between light and severe types, and the main direction of the transformation is consistent with the direction of the center of gravity migration (northeast and southwest). The severe and extremely severe gravity centers are shifting randomly because the areas of the two levels have relatively small changes, and the majority of the changes are mutual transformations between the two types.

3.2.2. Intensity analysis of desertification

Fig. 8 depicts the category intensity analysis results, and the category’s annual gain and loss intensities. The gain areas of the non-, lightly, and severely desertified lands were greater than the areas of loss, while the gain areas of the moderately and extremely severely desertified lands were smaller than the areas of loss during 1990–1995 (**Fig. 8a1**). In the gain analysis result for 1995, the gain intensities of the lightly, moderately, and severely desertified lands were active, while the non-desertified and extremely severely desertified lands were in a dormant state. In the loss analysis result (**Fig. 8a2**), only the light and moderate desertification lands were active. During 1995–2000, the gain areas of the lightly, moderately, and severely desertified lands were greater than the loss areas, and the changes were relatively active for these desertification levels. The gain areas of the non-desertified and severely desertified lands were less than the loss areas. The results indicate that under the same environmental conditions, moderately desertified land is the most sensitive to climate change and human activities. During 2000–2005, the gain areas of the moderately and severely desertified lands were greater than the loss areas, and the changes were relatively active for the two desertification levels. Among them, moderate desertification exhibited the most considerable change. During 2005–2010, the gain areas of the non-, lightly, severely, and extremely severely desertified lands were less than the loss areas, and the gain area of the moderately desertified land was approximately equal to the loss area. During 2010–2015, the gain area of the non-

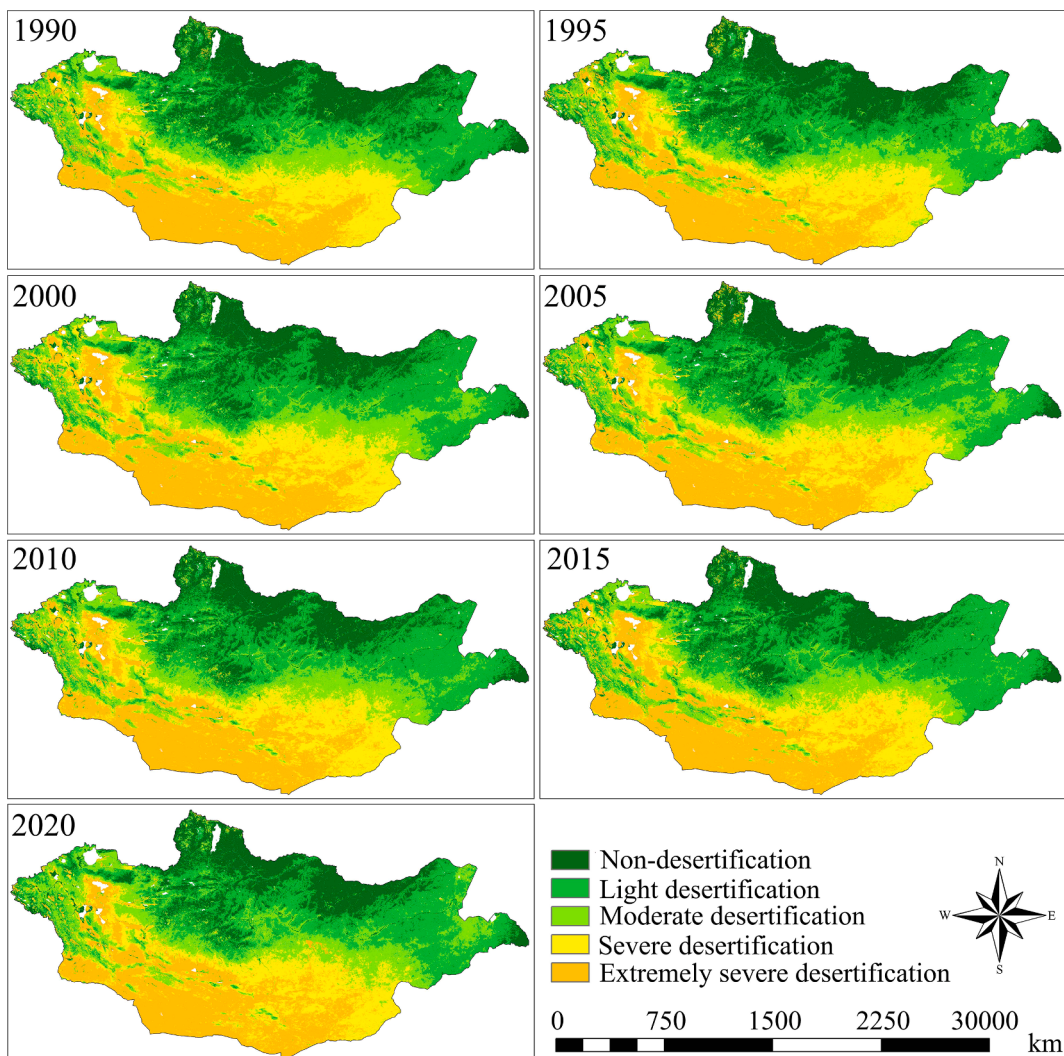


Fig. 6. Spatial distribution of desertification in Mongolia during 1990–2020.

desertified land was greater than the loss area, and the gain area of the extremely severely desertified land was approximately equal to the loss area. Excluding the extremely severely desertified land, all the levels of gains were active. During 2015–2020, the gain areas of the non-, moderate, and severe desertification categories were greater than the loss areas. The gain and loss trends in the moderate and severe desertification areas were more active. Among them, the moderate desertification area had the largest gain, and the light desertification area had the greatest losses. Collectively, desertified land generally increased from 1990 to 2020, which can be attributed to the decrease in the non-desertification area and increase in the moderate and severe desertification areas.

Table 2 presents the transition level analysis results. We enumerated the main levels of conversion in each level for each period. The non-desertification level for all periods was mainly converted into the light desertification level, and the total area of conversion reached 41,718 km². Light desertification was mainly converted into non-desertification and moderate desertification lands, with areas of 33,854 km² and 37,763 km², respectively. Moreover, the moderately desertified land are being mainly converted to severely desertified land during 2015–2020. However, during 1990–2015, the moderately desertified land was converted into light desertification land, with an area of 56,296 km². In summary, from the perspective of the main levels of conversion, moderately, severely, and extremely severely desertified lands have been reversed from 1990 to 2020. The deteriorated levels of

desertification are the original non-desertified and lightly desertified lands. The insights provide a scientific basis that could guide the formulation and implementation desertification prevention and control measures.

Fig. 9 shows the spatial distribution of the transition intensity between the types of desertification in Mongolia from 1990 to 2020. The areas with active desertification changes are mainly concentrated in the east of Mongolia. For example, the desertification in 2000–2005 and 2005–2010 were two diametrically opposed transitions, with exacerbation and reversal, respectively. In general, desertification transition types in Mongolia are mainly one-level conversions (such as light to moderate), and transition areas greater than one-level are very small.

3.3. Analysis of driving factors of desertification in Mongolia

In the present study, precipitation, VPD, PE, wind speed, elevation, number of livestock, soil type, slope degree, and slope aspect were used to analyze the factors driving the spatial distribution and area trends of desertification in Mongolia. Fig. 10 depicts the importance of each factor in the spatial distribution of desertification. Precipitation has the greatest influence on the spatial distribution of desertification, followed by VPD, PE, wind speed, and elevation. The number of livestock, soil type, slope, and aspect have little influence on the spatial distribution of desertification. Therefore, meteorological factors dominate the spatial distribution of desertification in Mongolia.

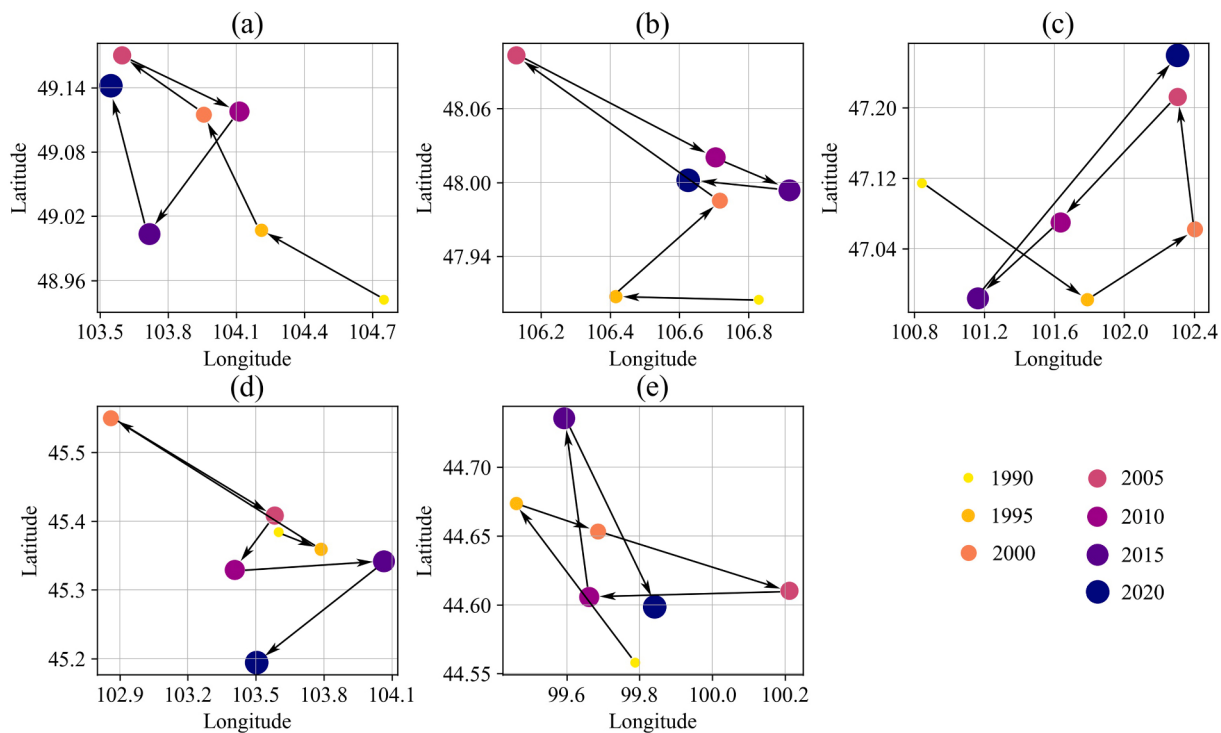


Fig. 7. Migration of the gravity center of different desertification categories. (a) None; (b) light; (c) moderate; (d) severe; and (e) extremely severe.

We selected precipitation, VPD, PE, wind speed, and livestock number to evaluate the forces driving change in desertification. The changes in each factor are depicted in Fig. 11. Precipitation in Mongolia has generally fluctuated and declined, with a decreasing rate of 1.11 mm yr^{-1} during 1990–2020. We used the segmented linear regression method (maximizing the sum of R^2 of two segments) (Yuan et al., 2019) to fit the precipitation and observed that 2005 was the mutation point of precipitation changes. Precipitation demonstrated a decreasing trend in 1990–2005 (-4.7 mm yr^{-1}) and a slightly increasing trend in 2005–2019 (1.8 mm yr^{-1}), which is opposite to the changes in the area of desertification in Mongolia, and indicates that the reversal of desertification in Mongolia after 2005 resulted from an increase in precipitation. The wind speed in Mongolia also demonstrates a downward trend in 1990–2020; however, the rate of decline is relatively slow (-0.004 m s^{-1}). Therefore, the change in wind speed did not promote desertification in Mongolia. The significant increases in the VPD, PET, and livestock number could also promote desertification land. In particular, the number of livestock has increased at a rate of 1,363 thousand heads per year, placing tremendous pressure on grassland resources.

4. Discussion

4.1. Desertification monitoring method on a large scale

Extracting nationwide high-resolution desertification information is essential for the formulation of timely desertification control measures and policies. The GEE, which is a platform for rapidly obtaining large-scale desertification information, provides a wealth of satellite data and classification methods for users. Although the GEE has been applied in many cartographic fields (Wu et al., 2019; Hird et al., 2017; Huang et al., 2017; Midekisa et al., 2017; Hansen et al., 2013), to the best of our knowledge, no such study relevant to monitoring desertification has been carried out based on the GEE platform. In the present study, we extracted desertification in Mongolia all over the country based on the GEE platform, and compared the performance of six machine learning methods in desertified land classification. We observed that the classification accuracy of the ME method was higher than those of the CART

(Xu et al., 2019; Liu et al., 2018) and RF methods (Belgiu and Drăguț, 2016). This provides a reference for the selection of classifiers in desertification classification research. In addition, in the indicator selection step, we used not only three common desertification indicators (e.g., MSAVI, Albedo, and TGS) (Duan et al., 2019; Liu et al., 2018; Lamchin et al., 2016), but also six bands (BLUE, GREEN, RED, NIR, SWIR1, and SWIR2) of Landsat images in the characteristic variables for training, which can be used as a supplement to the limited desertification indicators. In comparison with traditional visual interpretation (Hu et al., 2015; Xue et al., 2013) and automatic classification methods (Wang et al., 2020; Duan et al., 2019; Liu et al., 2018; Lamchin et al., 2016; Qi et al., 2012), this method has the advantages of high resolution, large area, long monitoring time, and high efficiency in desertification mapping.

4.2. Distinctions of desertification changes in Mongolia and China

Generally, the total area of desertified land in Mongolia has shown an obvious increasing trend, with a rate of increase of approximately $1,900 \text{ km}^2$ per year. Specifically, the area of desertification in Mongolia showed an increasing trend from 1990 to 2005, and decreased slightly after 2005. The light and moderate desertification areas showed the most rapidly expanding levels (Wang et al., 2019; Yu et al., 2013). Increasing desertification has directly affected the ecosystem of Mongolia and the neighboring regions (Lee et al., 2019; Filei et al., 2018; Garchinbyamba and Kang, 2013). According to the results of the present study, non-desertified land in northeastern Mongolia has been continuously converted into lightly desertified land in recent years. This requires the government to strengthen desertification control in the area, for instance, by formulating reasonable grazing management policies. China, which is extensively affected by desertification, has made great progresses in combating desertification (Duan et al., 2019; Zhang and Huisingsh, 2018). The area of desertified land in Inner Mongolia, which is consistent with Mongolia's geographical environment, has been declining in recent decades (Duan et al., 2019; Zhang and Huisingsh, 2018; Zhang et al., 2014). This is mainly because the Chinese government has successively implemented numerous ecological restoration

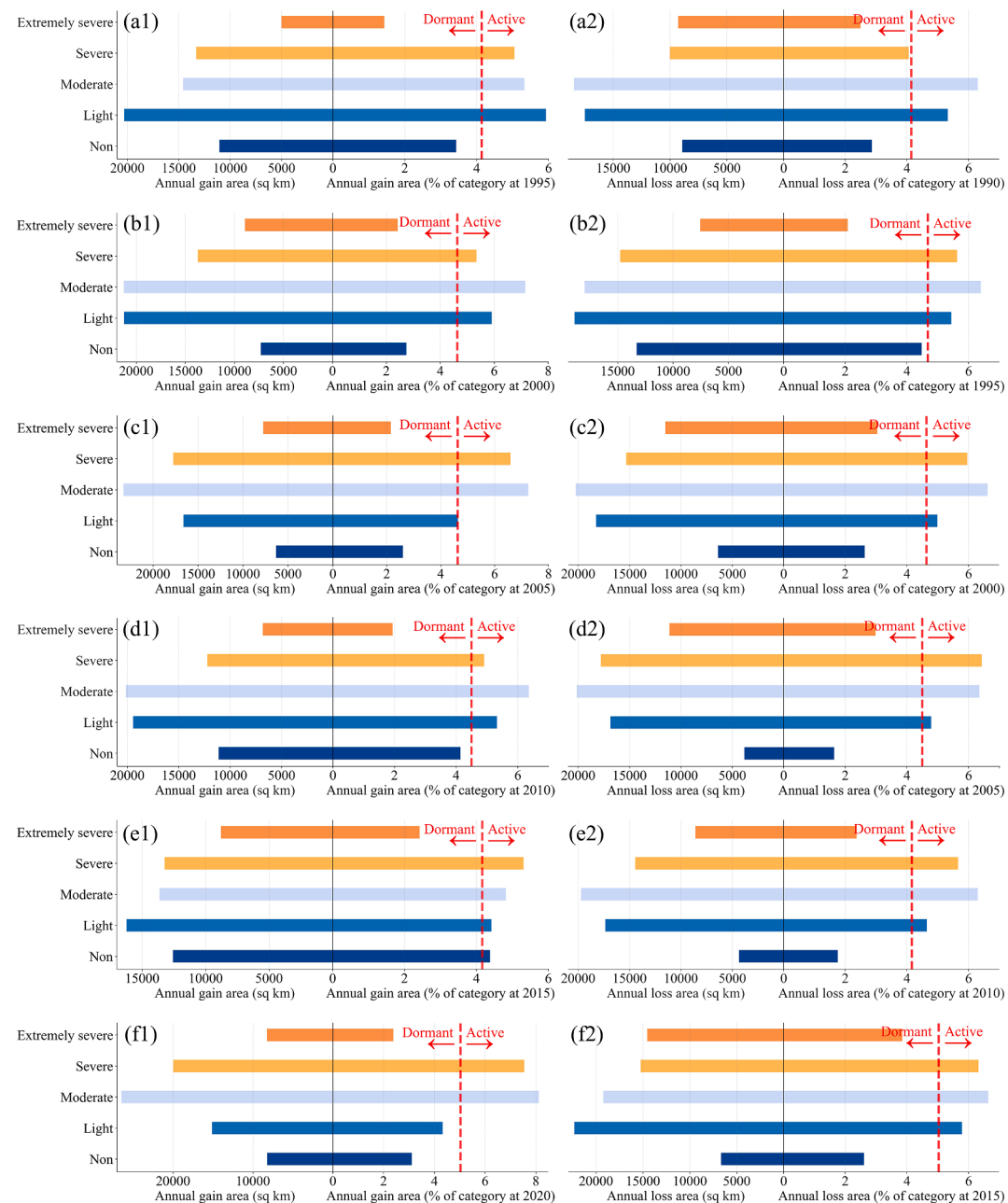


Fig. 8. Category intensity analysis for six stages. (a) 1990–1995; (b) 1995–2000; (c) 2000–2005; (d) 2005–2010; (e) 2010–2015; (f) 2015–2020; 1 and 2 represent gains and losses. The bar graph on the left of the zero axis represents the area of the annual gain of each category; the bar graph on the right of the zero axis represents the annual gain intensity of each category. If the intensity bar ends on the left side of the uniform line, the change in that category is relatively dormant during that interval. If the intensity bar extends to the right of the uniform line, the change in the category is relatively active during the time interval.

Table 2Major category conversions and areas (km^2) during different periods.

From category	To category						
		1990–1995	1995–2000	2000–2005	2005–2010	2010–2015	2015–2020
None	Category	Light	Light	Light	Light	Light	Light
	Area	8634	12,723	6061	3780	4185	6335
Light	Category	None	Moderate	Moderate	None	None	Moderate
	Area	10,718	11,646	11,954	10,654	12,482	14,163
Moderate	Category	Light	Light	Light	Light	Light	Severe
	Area	11,383	7975	9879	15,236	11,796	8859
Severe	Category	Moderate	Moderate	Moderate	Moderate	Moderate	Moderate
	Area	6329	7740	9057	11,715	7394	8608
Extremely severe	Category	Severe	Severe	Severe	Severe	Severe	Severe
	Area	7526	5527	9212	8405	6989	11,056

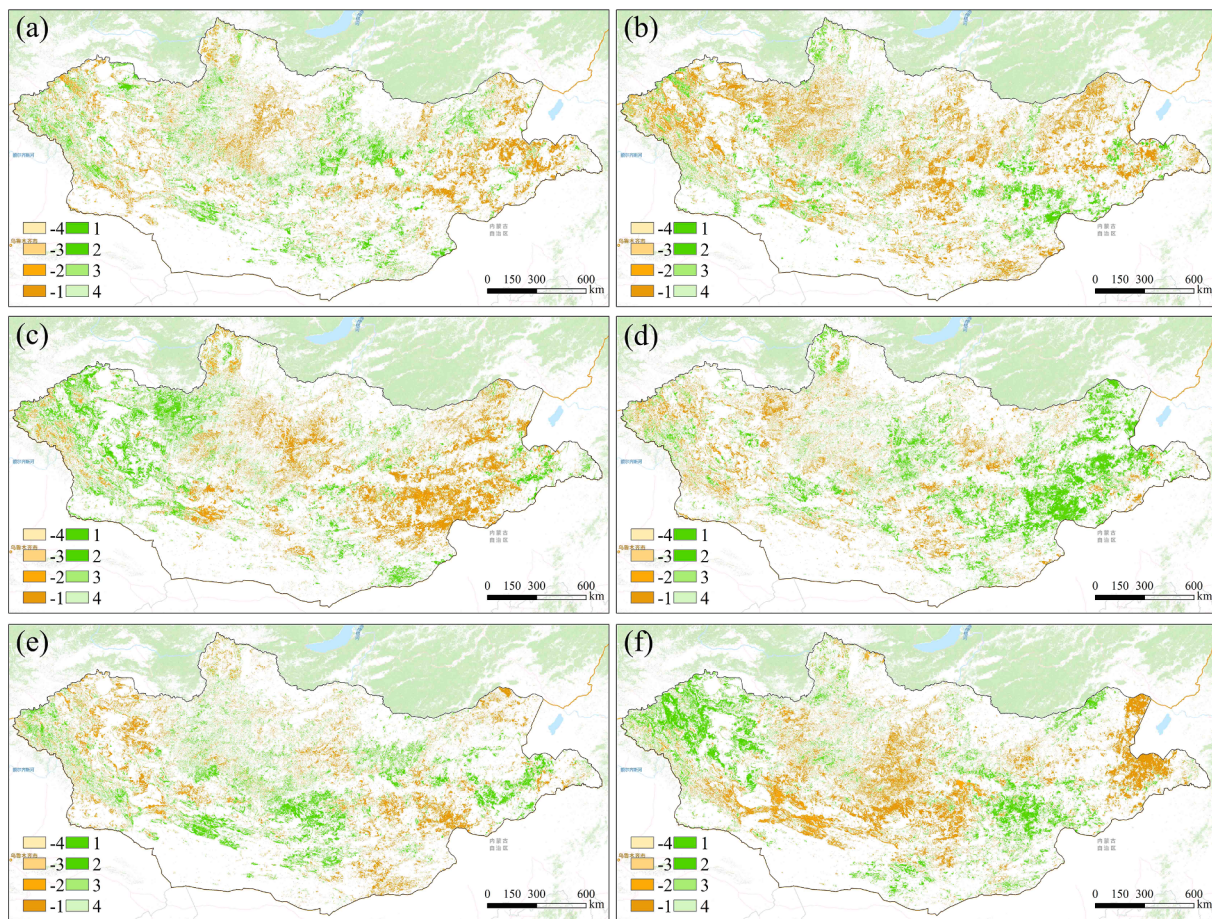


Fig. 9. Desertification degree category changes in Mongolia from 1990 to 2020. (a) 1990–1995; (b) 1995–2000; (c) 2000–2005; (d) 2005–2010; (e) 2010–2015; (f) 2015–2020. Here, -1 , -2 , -3 , and -4 represent the degrees aggravation of desertification, and the smaller the number, the greater the degree of aggravation is. 1 , 2 , 3 , and 4 indicate the degrees of desertification mitigation, and the greater the value, the greater the degree of desertification mitigation is.

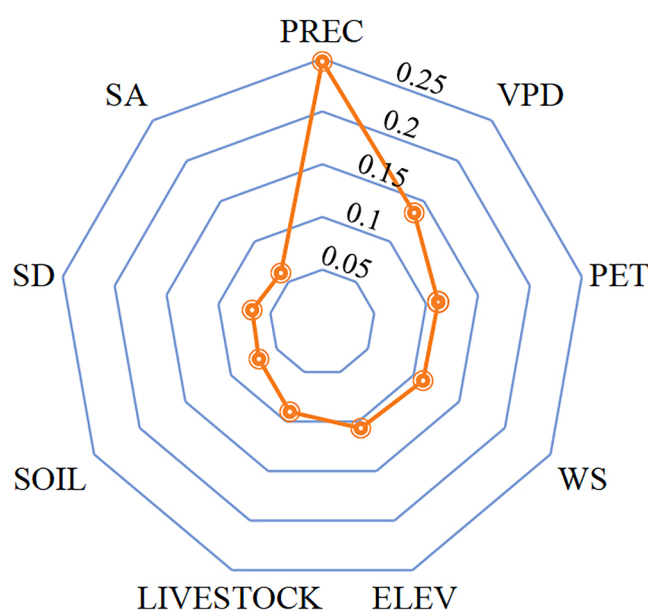


Fig. 10. Importance of factors affecting the influencing spatial distribution patterns of desertification in Mongolia. The order of importance of the factor order is as follows: precipitation (PREC) > vapor pressure deficit (VPD) > potential evapotranspiration (PET) and wind speed (WS) > elevation (ELEV) > number of livestock (LIVESTOCK) > soil type (SOIL) > slope degree (SD) > and slope aspect (SA).

policies since 1978, including the “Three North Shelterbelt Program,” “Combating of Desertification Program,” “Natural Forest Protection Project,” and “Grain for Green Project” (Jia et al., 2014; Wu et al., 2013), which have driven the reversal of desertification in northern China (Qi et al., 2012). Therefore, the desertification control experience in China, especially Inner Mongolia can provide a reference for Mongolia.

4.3. Driving factors of desertification in Mongolia

Climate change and human activities are two key factors influencing desertification dynamics (Ren et al., 2016; Lam et al., 2011). The factors driving desertification in different countries are diverse. For example, in northern China, government-led desertification prevention and control measures and ecological restoration projects play an important role in desertification trends (Liu et al., 2020; Zhang et al., 2020; Duan et al., 2019). In Kazakhstan, decrease in precipitation, increase in temperature, and high-intensity crop cultivation and animal husbandry activities are the key factors driving desertification (Hu et al., 2020; Jiang et al., 2019). Our results show that staged precipitation change is the major factor driving the development and reversal of desertification in Mongolia. The distributions of precipitation and desertified land in Mongolia are consistent. Spatially, less precipitation in southern Mongolia corresponds to extremely severely desertified land. The northern areas with more precipitation are dominated by lightly desertified and non-desertified lands. In terms of time, 2005 was the abrupt point of change in precipitation and desertification areas. Prior to 2005, the decrease in precipitation led to an increase in the area of desertification, while after 2005, the desertified land exhibited a

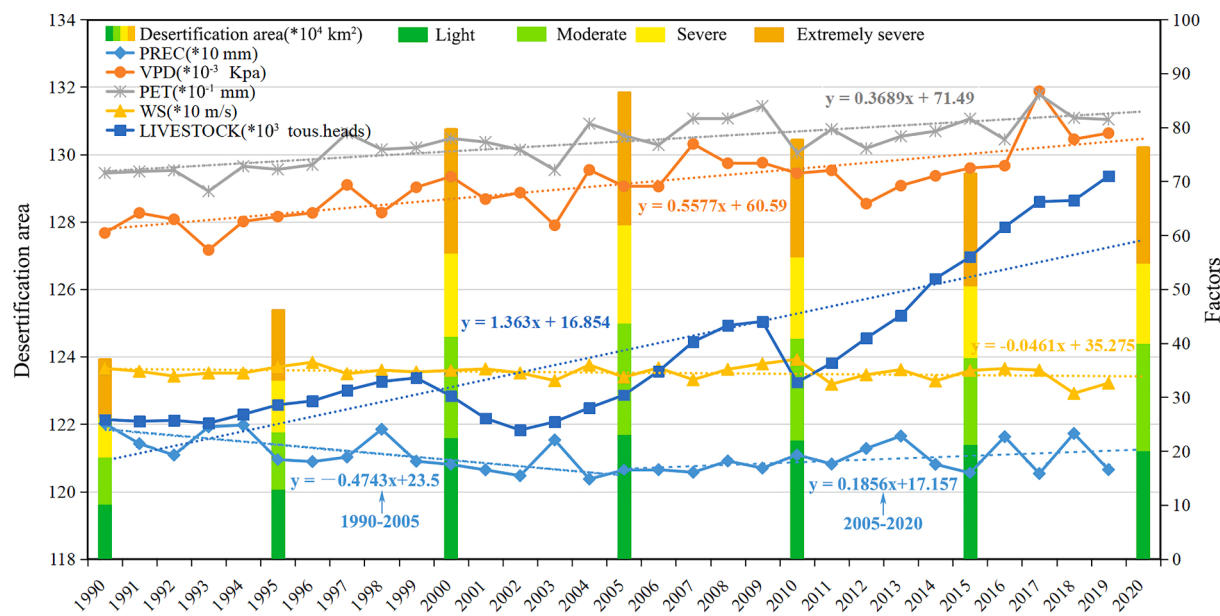


Fig. 11. Variations in desertification area, annual mean precipitation, vapor pressure deficit, potential evapotranspiration, wind speed, and livestock number in Mongolia during 1990–2020. Different colors indicate the proportions of different desertified land areas in separate histograms.

reversing trend due to a slight rebound in precipitation. This is consistent with the results obtained by Wang et al. (2017).

An increase in VPD increases the dryness of the air, which is not conducive to the growth of vegetation in Mongolia, exacerbating desertification. PE is the amount of evaporation and transpiration that occurs under sufficient water conditions (Prospero and Lamb, 2003), and PE is more representative of the vegetation growth environment than temperature (Zhang et al., 2020). The increase in PE has also promoted an increase in the desertification area. In general, our results reveal that a warm and dry climate is not conducive to the reversal of desertified land or maintenance and development of animal husbandry (Filei et al., 2018).

The impact of human activities on desertification is mainly manifested in the destruction of vegetation and increased surface exposure, which in turn leads to the loss of soil organic matter and degradation (D'Odorico et al., 2013). Owing to the regime change in the 1990s, the society adopted a market economy, and land is now owned by the herders (Sheng et al., 2000). Driven by the market economy, the number of livestock increased significantly from 1990 to 2020. This has further increased the pressure on pasture resources, leading to an increase in the area of desertified land (Zolotokrylin et al., 2016). However, Fig. 11 shows that there was no significant consistency between the changes in the desertification area and the number of livestock after 2005, which may be because the impact of the number of livestock on the area of desertified land can be neglected in comparison with precipitation (Fig. 10). In addition, as illustrated in Fig. 4h, grazing is mainly concentrated in the central part of Mongolia, with a small amount in the east. However, according to Fig. 9, the areas with aggravated desertification are mainly concentrated in the eastern part of Mongolia, which is obviously not consistent with the distribution of heavily grazed areas.

Desertification development is sensitive to changes in precipitation. To combat desertification, the Mongolian government has cooperated with neighboring countries and conducted a series of ecological restoration and desertification control measures and projects (Kang et al., 2010). Such measures have reversed desertification to a certain extent, even if the reversals have been limited to local areas. Considering the warm and dry climate and an increase in the number of livestock in Mongolia, desertification is expected to continue to threaten the ecological environment. We recommend that effective ecological restoration measures need to continue to be implemented.

5. Conclusions

Land desertification dynamics influence the development of Mongolia's ecological environment and animal husbandry. In the present study, a desertification map of Mongolia from 1990 to 2020 was produced based on the GEE platform and various machine learning methods. The desertification mapping could provide a reference for Mongolia to formulate timely desertification control policies and measures.

Based on an analysis of the temporal and spatial characteristics of different types of desertified land areas in Mongolia from 1990 to 2020, 2005 was found to be the turning point for Mongolia's desertified land area, where it shifted from an increasing trend to a decreasing trend. In addition, according to the results, land with non-desertification continues to decrease, light and moderate desertification lands are the major increasing types, and the areas of severe and extremely severe desertification lands have not changed significantly. The eastern part of Mongolia has the highest transformation intensity among different types. Precipitation was the dominant factor influencing not only the spatial distribution of desertification but also the desertification trends. In addition, increases in evapotranspiration and grazing intensity have exacerbated land desertification. National government ecological restoration measures are vital for the reversal of local desertified land. The impacts of climate warming and humidification on desertification in Mongolia are relatively complex. An increase in precipitation would influence future desertification trends more than an increase in potential evapotranspiration. We suggest that Mongolia's desertification prevention and control strategies focus on preventing continuous degradation of non-desertified land in the north of the country, and rationally manage grazing on the lightly and moderately desertified lands. In the case of severely and extremely severely desertified lands, particularly sites that are inhabited by humans, the government should continuously implement ecological restoration projects and desertification control measures.

CRediT authorship contribution statement

Xiaoyu Meng: Conceptualization, Data curation, Methodology, Writing - original draft. **Xin Gao:** Conceptualization, Methodology, Writing - review & editing. **Sen Li:** Methodology. **Shengyu Li:**

Visualization. Jiaqiang Lei: Investigation.

Declaration of Competing Interest

The authors declare that they have no known competing financial interests or personal relationships that could have appeared to influence the work reported in this paper.

Acknowledgements

We are grateful to the members of the Institute of Geography & Geoecology, Mongolian Academy of Sciences for their field work support.

Funding: This research was funded by the project of Research and Development of Sand Prevention Technology of Highway and Soil Erosion Control Technology of Pipelines, an important part of the Strategic Priority Research Program of the Chinese Academy of Sciences (Class A) - The Pan-Third-Pole Environmental Change and Green Silk Road Construction (grant number XDA2003020201), the Strategic Priority Research Program of Chinese Academy of Sciences, Pan-Third Pole Environment Study for a Green Silk Road (Pan-TPE) (grant number XDA2009000001), the National Key Research and Development Program of China-Mongolia cooperation research and demonstration in grassland desertification control technology (grant number 2017YFE0109200) and the China-initiated “Belt and Road Special Project” (grant number 131965KYSB20170038).

References

- Abatzoglou, J.T., Dobrowski, S.Z., Parks, S.A., Hegewisch, K.C., 2018. TerraClimate, a high-resolution global dataset of monthly climate and climatic water balance from 1958–2015. *Sci. Data* 5, 170191. <https://doi.org/10.1038/sdata.2017.191>.
- Aldwaik, S.Z., Pontius, R.G., 2012. Intensity analysis to unify measurements of size and stationarity of land changes by interval, category, and transition. *Landscape Urban Plann.* 106 (1), 103–114. <https://doi.org/10.1016/j.landurbplan.2012.02.010>.
- Arabameri, A., Asadi Nalivan, O., Saha, S., Roy, J., Pradhan, B., Tiefenbacher, J.P., Thi Ngo, P.T., 2020. Novel ensemble approaches of machine learning techniques in modeling the gully erosion susceptibility. *Remote Sensing* 12, 1890. <https://doi.org/10.3390/rs12111890>.
- Banko, G., 1998. A review of assessing the accuracy of classifications of remotely sensed data and of methods including remote sensing data in forest inventory. IIASA Interim Report.
- Belgiu, M., Drăguț, L., 2016. Random forest in remote sensing: a review of applications and future directions. *ISPRS J. Photogramm. Remote Sens.* 114, 24–31. <https://doi.org/10.1016/j.isprsjprs.2016.01.011>.
- Zou, Z., Xiao, X., Dong, J., Qian, Y., Doughty, R.B., 2018. Divergent trends of open-surface water body area in the contiguous United States from 1984 to 2016. *Proc. Natl. Acad. Sci.* 115, 3810–3815. <https://doi.org/10.1073/pnas.1719275115>.
- Bespakov, N.D., 1964. Soils of Outer Mongolia (Mongolian People's Republic) Pochvy Mongol'skoi Narodnoi Respublikii. Israel Program for Scientific Translations; [available from the Office of Technical Services, U.S. Department of Commerce, Washington].
- Bezerra, F.G.S., Aguiar, A.P.D., Alvalá, R.C.S., Giarolla, A., Bezerra, K.R.A., Lima, P.V.P. S., do Nascimento, F.R., Arai, E., 2020. Analysis of areas undergoing desertification, using EVI2 multi-temporal data based on MODIS imagery as indicator. *Ecol. Ind.* 117, 106579. <https://doi.org/10.1016/j.ecolind.2020.106579>.
- Bofana, J., Zhang, M., Nabil, M., Wu, B., Tian, F., Liu, W., Zeng, H., Zhang, N., Nangombe, S.S., Cipriano, S.A., Phiri, E., Mushore, T.D., Kaluba, P., Mashonjowa, E., Moyo, C., 2020. Comparison of different cropland classification methods under diversified agroecological conditions in the Zambezi River Basin. *Remote Sens.* 12, 2096. <https://doi.org/10.3390/rs12132096>.
- Breiman, L., 2001. Random forests. *Mach. Learn.* 45, 5–32. <https://doi.org/10.1023/A:1010933404324>.
- Chan, J.-W., Paclincx, D., 2008. Evaluation of Random Forest and Adaboost tree-based ensemble classification and spectral band selection for ecotope mapping using airborne hyperspectral imagery. *Remote Sens. Environ.* 112 (6), 2999–3011. <https://doi.org/10.1016/j.rse.2008.02.011>.
- Chen, T.-H., Qiu, C., Schmitt, M., Zhu, X.X., Sabel, C.E., Prishchepov, A.V., 2020. Mapping horizontal and vertical urban densification in Denmark with Landsat time-series from 1985 to 2018: a semantic segmentation solution. *Remote Sens. Environ.* 251, 112096. <https://doi.org/10.1016/j.rse.2020.112096>.
- Congalton, R.G., 1991. A review of assessing the accuracy of classifications of remotely sensed data. *Remote Sen. Environ.* 37 (1), 35–46. [https://doi.org/10.1016/0034-4257\(91\)90048-B](https://doi.org/10.1016/0034-4257(91)90048-B).
- Congalton, R.G., Green, K., Green, K., 2008. Assessing the Accuracy of Remotely Sensed Data : Principles and Practices, 2nd ed. CRC Press. <https://doi.org/10.1201/9781420055139>.
- D'Odorico, P., Bhattachan, A., Davis, K.F., Ravi, S., Runyan, C.W., 2013. Global desertification: drivers and feedbacks. *Advances in water resources. 35th Year Anniversary Issue* 51, 326–344. <https://doi.org/10.1016/j.advwatres.2012.01.013>.
- Dorj, O., Enkhbold, M., Ikhbayanjin, S., Mijiddorj, K.h., Nosmoo, A., Puntsagnamil, M., Sainjargal, U., 2013. Mongolia: country features, the main causes of desertification and remediation efforts. In: Heshmati, G.A., Squires, V.R. (Eds.), Combating Desertification in Asia, Africa and the Middle East: Proven Practices. Springer, Netherlands, Dordrecht, pp. 217–229. https://doi.org/10.1007/978-94-007-6652-5_11.
- Duan, H., Wang, T., Xue, X., Yan, C., 2019. Dynamic monitoring of aeolian desertification based on multiple indicators in Horqin Sandy Land, China. *Sci. Total Environ.* 650, 2374–2388. <https://doi.org/10.1016/j.scitotenv.2018.09.374>.
- Dwyer, J.L., Roy, D.P., Sauer, B., Jenkinson, C.B., Zhang, H.K., Lymburner, L., 2018. Analysis ready data: enabling analysis of the landsat archive. *Remote Sens.* 10, 1363. <https://doi.org/10.3390/rs10091363>.
- Eckert, S., Hüslér, F., Liniger, H., Hodel, E., 2015. Trend analysis of MODIS NDVI time series for detecting land degradation and regeneration in Mongolia. *J. Arid Environ.* 113, 16–28. <https://doi.org/10.1016/j.jaridenv.2014.09.001>.
- Elith, J., Phillips, S.J., Hastie, T., Dudík, M., Chee, Y.E., Yates, C.J., 2011. A statistical explanation of MaxEnt for ecologists. *Divers. Distrib.* 17, 43–57. <https://doi.org/10.1111/j.1472-4642.2010.00725.x>.
- Filei, A.A., Slesarenko, L.A., Boroditskaya, A.V., Mishigdorj, O., 2018. Analysis of desertification in Mongolia. *Russ. Meteorol. Hydrol.* 43 (9), 599–606. <https://doi.org/10.3103/S1068373918090066>.
- Foody, G.M., 2002. Status of land cover classification accuracy assessment. *Remote Sens. Environ.* 80 (1), 185–201. [https://doi.org/10.1016/S0034-4257\(01\)00295-4](https://doi.org/10.1016/S0034-4257(01)00295-4).
- Friedl, M.A., McIver, D.K., Hodges, J.C.F., Zhang, X.Y., Muchoney, D., Strahler, A.H., Woodcock, C.E., Gopal, S., Schneider, A., Cooper, A., Baccini, A., Gao, F., Schaaf, C., 2002. Global land cover mapping from MODIS: algorithms and early results. *Remote Sensing of Environment*, The Moderate Resolution Imaging Spectroradiometer (MODIS): a new generation of Land Surface Monitoring 83, 287–302. [https://doi.org/10.1016/S0034-4257\(02\)00078-0](https://doi.org/10.1016/S0034-4257(02)00078-0).
- Garchinbyamba, M., Kang, H., 2013. Analyzing causes of desertification in Bayankhangai soum, Tuv province, central Mongolia. *Forest Science and Technology* 9 (2), 59–64. <https://doi.org/10.1080/21580103.2012.761946>.
- Gorelick, N., Hancher, M., Dixon, M., Ilyushchenko, S., Thau, D., Moore, R., 2017. Google earth engine: planetary-scale geospatial analysis for everyone. *Remote Sens. Environ.* Big Remotely Sensed Data: Tools, Applications Experiences 202, 18–27. <https://doi.org/10.1016/j.rse.2017.06.031>.
- Gregoretto, B., Michel, B., Saint-Pierre, P., 2017. Correlation and variable importance in random forests. *Stat. Comput.* 27 (3), 659–678. <https://doi.org/10.1007/s11222-016-9646-1>.
- Guo, B., Zang, W., Han, B., Yang, F., Luo, W., He, T., Fan, Y., Yang, X., Chen, S., 2020. Dynamic monitoring of desertification in Naiman Banner based on feature space models with typical surface parameters derived from LANDSAT images. *Land Degrad. Dev.* n/a 31 (12), 1573–1592. <https://doi.org/10.1002/lrd.v31.1210.1002/lrd.3533>.
- Gustafsson, M.G., Wallman, M., Wickenberg Bolin, U., Göransson, H., Fryknäs, M., Andersson, C.R., Isaksson, A., 2010. Improving Bayesian credibility intervals for classifier error rates using maximum entropy empirical priors. *Artif. Intell. Med.* 49 (2), 93–104. <https://doi.org/10.1016/j.artmed.2010.02.004>.
- Han, Z., Wang, T., Yan, C., Liu, Y., Liu, L., Li, A., Du, H., 2010. Change trends for desertified lands in the Horqin Sandy Land at the beginning of the twenty-first century. *Environ. Earth Sci.* 59 (8), 1749–1757. <https://doi.org/10.1007/s12665-009-0157-7>.
- Hansen, M.C., Potapov, P.V., Moore, R., Hancher, M., Turubanova, S.A., Tyukavina, A., Thau, D., Stehman, S.V., Goetz, S.J., Loveland, T.R., Kommareddy, A., Egorov, A., Chini, L., Justice, C.O., Townshend, J.R.G., 2013. High-resolution global maps of 21st-century forest cover change. *Science* 342 (6160), 850–853. <https://doi.org/10.1126/science:1244693>.
- Hird, J.N., DeLancey, E.R., McDermid, G.J., Kariyeva, J., 2017. Google earth engine, open-access satellite data, and machine learning in support of large-area probabilistic wetland mapping. *Remote Sens.* 9, 1315. <https://doi.org/10.3390/rs9121315>.
- Hu, G., Dong, Z., Lu, J., Yan, C., 2015. The developmental trend and influencing factors of aeolian desertification in the Zoige Basin, eastern Qinghai-Tibet Plateau. *Aeolian Res. Eighth Int. Conf. Aeolian Res. – ICAR* 8 19, 275–281. <https://doi.org/10.1016/j.aeolia.2015.02.002>.
- Hu, Y., Han, Y., Zhang, Y., 2020. Land desertification and its influencing factors in Kazakhstan. *J. Arid Environ.* 180, 104203. <https://doi.org/10.1016/j.jaridenv.2020.104203>.
- Huang, H., Chen, Y., Clinton, N., Wang, J., Wang, X., Liu, C., Gong, P., Yang, J., Bai, Y., Zheng, Y., Zhu, Z., 2017. Mapping major land cover dynamics in Beijing using all Landsat images in Google Earth Engine. *Remote Sens. Environ.* Big Remotely Sensed Data: Tools, Applications Experiences 202, 166–176. <https://doi.org/10.1016/j.rse.2017.02.021>.
- Izquierdo-Verdúguier, E., Zurita-Milla, R., 2020. An evaluation of Guided Regularized Random Forest for classification and regression tasks in remote sensing. *Int. J. Appl. Earth Obs. Geoinf.* 88, 102051. <https://doi.org/10.1016/j.jag.2020.102051>.
- Jia, X., Fu, B., Feng, X., Hou, G., Liu, Y., Wang, X., 2014. The tradeoff and synergy between ecosystem services in the Grain-for-Green areas in Northern Shaanxi, China. *Ecol. Ind.* 43, 103–113. <https://doi.org/10.1016/j.ecolind.2014.02.028>.
- Jiang, L., Jiapaer, G., Bao, A., Kurban, A., Guo, H., Zheng, G., De Maeyer, P., 2019. Monitoring the long-term desertification process and assessing the relative roles of its drivers in Central Asia. *Ecol. Ind.* 104, 195–208. <https://doi.org/10.1016/j.ecolind.2019.04.067>.

- Joshi, P.P., Wynne, R.H., Thomas, V.A., 2019. Cloud detection algorithm using SVM with SWIR2 and tasseled cap applied to Landsat 8. *Int. J. Appl. Earth Obs. Geoinf.* 82, 101898. <https://doi.org/10.1016/j.jag.2019.101898>.
- Jugder, D., Shinoda, M., Sugimoto, N., Matsui, I., Nishikawa, M., Park, S.-U., Chun, Y.-S., Park, M.-S., 2011. Spatial and temporal variations of dust concentrations in the Gobi Desert of Mongolia. *Global Planet. Change* 78 (1-2), 14–22. <https://doi.org/10.1016/j.gloplacha.2011.05.003>.
- Jy, S., Mz, L., Lh, Z., Yg, H., Xj, Z., 2006. Real-time analysis of soil moisture, soil organic matter, and soil total nitrogen with NIR spectra. *Guang Pu Xue Yu Guang Pu Fen Xi* 26, 426–429.
- Kang, M.K., Park, D.K., Chun, Y.W., 2010. The performance analysis of Korean NGOs' tree plantation projects in Mongolia. *J. Korean For. Soc.* 99, 655–662.
- Kimura, R., Shinoda, M., 2010. Spatial distribution of threshold wind speeds for dust outbreaks in northeast Asia. *Geomorphology* 114 (3), 319–325. <https://doi.org/10.1016/j.geomorph.2009.07.014>.
- Lam, D.K., Remmell, T.K., Drezner, T.D., 2011. Tracking desertification in California using remote sensing: a sand dune encroachment approach. *Remote Sens.* 3, 1–13. <https://doi.org/10.3390/rs3010001>.
- Lamchin, M., Lee, J.-Y., Lee, W.-K., Lee, E.J., Kim, M., Lim, C.-H., Choi, H.-A., Kim, S.-R., 2016. Assessment of land cover change and desertification using remote sensing technology in a local region of Mongolia. *Adv. Space Res.* 57 (1), 64–77. <https://doi.org/10.1016/j.asr.2015.10.006>.
- Landkriet, S., Asfaha, T., Frankl, A., Zenebe, A., Nyssen, J., 2016. Sediment in alluvial and lacustrine debris fans as an indicator for land degradation around Lake Ashenge (Ethiopia). *Land Degrad. Dev.* 27 (2), 258–269. <https://doi.org/10.1002/ldr.2424>.
- Lee, E.J., Piao, D., Song, C., Kim, J., Lim, C.-H., Kim, E., Moon, J., Kafatos, M., Lamchin, M., Jeon, S.W., Lee, W.-K., 2019. Assessing environmentally sensitive land to desertification using MEDALUS method in Mongolia. *For. Sci. Technol.* 15 (4), 210–220. <https://doi.org/10.1080/21580103.2019.1667804>.
- Li, W., Dong, R., Fu, H., Wang, J., Yu, L.e., Gong, P., 2020a. Integrating Google Earth imagery with Landsat data to improve 30-m resolution land cover mapping. *Remote Sens. Environ.* 237, 111563. <https://doi.org/10.1016/j.rse.2019.111563>.
- Li, X., Gong, P., Zhou, Y., Wang, J., Bai, Y., Chen, B., Hu, T., Xiao, Y., Xu, B., Yang, J., Liu, X., Cai, W., Huang, H., Wu, T., Wang, X.i., Lin, P., Li, X., Chen, J., He, C., Li, X., Yu, L.e., Clinton, N., Zhu, Z., 2020b. Mapping global urban boundaries from the global artificial impervious area (GALA) data. *Environ. Res. Lett.* 15 (9), 094044. <https://doi.org/10.1088/1748-9326/ab9be3>.
- Liang, S., 2001. Narrowband to broadband conversions of land surface albedo I: Algorithms. *Remote Sens. Environ.* 76 (2), 213–238. [https://doi.org/10.1016/S0034-4257\(00\)00205-4](https://doi.org/10.1016/S0034-4257(00)00205-4).
- Liau, A., Wiener, M., 2002. Classification and regression with random forest. *R News* 23, 23.
- Lin, M., Chu, C., Shih, J., 2006. Assessment and monitoring of desertification using satellite imagery of MODIS in East Asia. *Agric. Hydrol. Applications Remote Sens.* 6411 <https://doi.org/10.1117/12.693920>.
- Liu, Q., Liu, G., Huang, C., 2018. Monitoring desertification processes in Mongolian Plateau using MODIS tasseled cap transformation and TGS1 time series. *J. Arid Land* 10 (1), 12–26. <https://doi.org/10.1007/s40333-017-0109-0>.
- Liu, Q., Zhang, Q., Yan, Y., Zhang, X., Niu, J., Svenning, J.-C., 2020. Ecological restoration is the dominant driver of the recent reversal of desertification in the Mu Us Desert (China). *J. Cleaner Prod.* 268, 122241. <https://doi.org/10.1016/j.jclepro.2020.122241>.
- Lu, D., Mausel, P., Batistella, M., Moran, E., 2004. Comparison of Land-Cover Classification Methods in the Brazilian Amazon Basin. *Photogramm. Eng. Remote Sens.* 70 (6), 723–731. <https://doi.org/10.14358/PERS.70.6.723>.
- Ma, H., Zhao, H., 1994. United Nations: convention to combat desertification in those countries experiencing serious drought and/or desertification, particularly in Africa. *Int. Legal Mater* 1328–1382.
- Meng, X., Gao, X., Li, S., Lei, J., 2020. Spatial and temporal characteristics of vegetation NDVI changes and the driving forces in Mongolia during 1982–2015. *Remote Sens.* 12, 603. <https://doi.org/10.3390/rs12040603>.
- Midekisa, A., Holl, F., Savory, D.J., Andrade-Pacheco, R., Gething, P.W., Bennett, A., Sturrock, H.J.W., Schumann, G.-P., 2017. Mapping land cover change over continental Africa using Landsat and Google Earth Engine cloud computing. *PLoS ONE* 12 (9), e0184926. <https://doi.org/10.1371/journal.pone.0184926>. <https://doi.org/10.1371/journal.pone.0184926.g0011>. <https://doi.org/10.1371/journal.pone.0184926.g0021>. <https://doi.org/10.1371/journal.pone.0184926.g0041>. <https://doi.org/10.1371/journal.pone.0184926.g0061>. <https://doi.org/10.1371/journal.pone.0184926.g0071>. <https://doi.org/10.1371/journal.pone.0184926.g0081>. <https://doi.org/10.1371/journal.pone.0184926.t002>.
- Miranda, J.d.R., Alves, M.d.C., Pozza, E.A., Santos Neto, H., 2020. Detection of coffee berry necrosis by digital image processing of landsat 8 oli satellite imagery. *Int. J. Appl. Earth Obs. Geoinf.* 85, 101983. <https://doi.org/10.1016/j.jag.2019.101983>.
- Na, R., Du, H., Na, L.i., Shan, Y., He, H.S., Wu, Z., Zong, S., Yang, Y., Huang, L., 2019. Spatiotemporal changes in the Aeolian desertification of Hulunbuir Grassland and its driving factors in China during 1980–2015. *CATENA* 182, 104123. <https://doi.org/10.1016/j.catena.2019.104123>.
- Pekel, J.-F., Cottam, A., Gorelick, N., Belward, A.S., 2016. High-resolution mapping of global surface water and its long-term changes. *Nature* 540 (7633), 418–422. <https://doi.org/10.1038/nature20584>.
- Phillips, S.J., Dudík, M., Elith, J., Graham, C.H., Lehmann, A., Leathwick, J., Ferrier, S., 2009. Sample selection bias and presence-only distribution models: implications for background and pseudo-absence data. *Ecol. Appl.* 19 (1), 181–197. <https://doi.org/10.1890/07-2153.1>.
- Prospero, J.M., Lamb, P.J., 2003. African droughts and dust transport to the Caribbean: climate change implications. *Science* 302, 1024–1027. <https://doi.org/10.1126/science.1089915>.
- Qi, J., Chehbouni, A., Huete, A.R., Kerr, Y.H., Sorooshian, S., 1994. A modified soil adjusted vegetation index. *Remote Sens. Environ.* 48 (2), 119–126. [https://doi.org/10.1016/0034-4257\(94\)90134-1](https://doi.org/10.1016/0034-4257(94)90134-1).
- Qi, Y., Chang, Q., Jia, K., Liu, M., Liu, J., Chen, T., 2012. Temporal-spatial variability of desertification in an agro-pastoral transitional zone of northern Shaanxi Province, China. *CATENA* 88 (1), 37–45. <https://doi.org/10.1016/j.catena.2011.08.003>.
- Rasmussen, K., Fog, B., Madsen, J.E., 2001. Desertification in reverse? Observations from northern Burkina Faso. *Global Environ. Change* 11 (4), 271–282. [https://doi.org/10.1016/S0959-3780\(01\)00005-X](https://doi.org/10.1016/S0959-3780(01)00005-X).
- Ren, X., Dong, Z., Hu, G., Zhang, D., Li, Q., 2016. A GIS-Based assessment of vulnerability to aeolian desertification in the source areas of the Yangtze and Yellow Rivers. *Remote Sens.* 8, 626. <https://doi.org/10.3390/rs8080626>.
- Robinove, C.J., Chavez, P.S., Gehring, D., Holmgren, R., 1981. Arid land monitoring using Landsat albedo difference images. *Remote Sens. Environ.* 11, 133–156. [https://doi.org/10.1016/0034-4257\(81\)90014-6](https://doi.org/10.1016/0034-4257(81)90014-6).
- Sanzheev, E.D., Mikheeva, A.S., Osodoev, P.V., Batomunkuev, V.S., Tulokhonov, A.K., 2020. Theoretical approaches and practical assessment of socio-economic effects of desertification in Mongolia. *Int. J. Environ. Res. Public Health* 17, 4068. <https://doi.org/10.3390/ijerph17114068>.
- Shannon, C.E., 1948. A mathematical theory of communication. *Bell Syst. Tech. J.* 27, 379–423. <https://doi.org/10.1002/j.1538-7305.1948.tb01338.x>.
- Shelestov, A., Lavreniuk, M., Kussul, N., Novikov, A., Skakun, S., 2017. Exploring google earth engine platform for big data processing: classification of multi-temporal satellite imagery for crop mapping. *Front. Earth Sci.* 5 <https://doi.org/10.3389/feart.2017.00017>.
- Sheng, G., Harazono, Y., Oikawa, T., Zhao, H.L., Ying He, Z., Chang, X.L., 2000. Grassland desertification by grazing and the resulting micrometeorological changes in Inner Mongolia. *Agric. For. Meteorol.* 102, 125–137. [https://doi.org/10.1016/S0168-1923\(00\)00105-1](https://doi.org/10.1016/S0168-1923(00)00105-1).
- Spinoni, J., Vogt, J., Naumann, G., Carrao, H., Barbosa, P., 2015. Towards identifying areas at climatological risk of desertification using the Köppen-Geiger classification and FAO aridity index. *Int. J. Climatol.* 35 (9), 2210–2222. [https://doi.org/10.1002/joc.4124](https://doi.org/10.1002/joc.2015.35.issue-910.1002/joc.4124).
- Tang, X., Li, J., Liu, M., Liu, W., Hong, H., 2020. Flood susceptibility assessment based on a novel random Naïve Bayes method: a comparison between different factor discretization methods. *CATENA* 190, 104536. <https://doi.org/10.1016/j.catena.2020.104536>.
- Teluguntla, P., Thenkabail, P.S., Oliphant, A., Xiong, J., Gumma, M.K., Congalton, R.G., Yadav, K., Huete, A., 2018. A 30-m landsat-derived cropland extent product of Australia and China using random forest machine learning algorithm on Google Earth Engine cloud computing platform. *ISPRS J. Photogramm. Remote Sens.* 144, 325–340. <https://doi.org/10.1016/j.isprsjprs.2018.07.017>.
- Vapnik, V.N. (Ed.), 2000. *The Nature of Statistical Learning Theory*. Springer New York, New York, NY.
- Verstraete, M.M., 1989. Land surface processes in climate models: status and prospects. In: Berger, A., Schneider, S., Duplessy, J.Cl. (Eds.), *Climate and Geo-Sciences: A Challenge for Science and Society in the 21st Century*, NATO ASI Series. Springer Netherlands, Dordrecht, pp. 321–340. <https://doi.org/10.1007/978-94-009-2446-8-18>.
- Wang, J., Cheng, K., Liu, Q., Zhu, J., Ochir, A., Davaasuren, D., Li, G., Wei, H., Chonokhuu, S., Namsrai, O., Bat-Erdene, A., 2019. Land cover patterns in Mongolia and their spatiotemporal changes from 1990 to 2010. *Arab. J. Geosci.* 12, 778. <https://doi.org/10.1007/s12517-019-4893-z>.
- Wang, J., Wei, H., Cheng, K., Ochir, A., Davaasuren, D., Li, P., Shun Chan, F.K., Nasanbat, E., 2020. Spatio-temporal pattern of land degradation from 1990 to 2015 in Mongolia. *Environ. Dev. Resour. Use Ecosyst. Restor. Green Dev.* 34, 100497. <https://doi.org/10.1016/j.envdev.2020.100497>.
- Wang, X., Hua, T., Lang, L., Ma, W., 2017. Spatial differences of aeolian desertification responses to climate in arid Asia. *Global Planet. Change* 148, 22–28. <https://doi.org/10.1016/j.gloplacha.2016.11.008>.
- Wei, H., Wang, J., Cheng, K., Li, G., Ochir, A., Davaasuren, D., Chonokhuu, S., 2018. Desertification information extraction based on feature space combinations on the Mongolian Plateau. *Remote Sens.* 10, 1614. <https://doi.org/10.3390/rs10101614>.
- Wei, H., Wang, J., Han, B., 2020. Desertification information extraction along the China-Mongolia Railway supported by multisource feature space and geographical Zoning modeling. *IEEE J. Sel. Top. Appl. Earth Obs. Remote Sens.* 13, 392–402. <https://doi.org/10.1109/JSTARS.460944310.1109/JSTARS.2019.2962830>.
- Wu, Q., Lane, C.R., Li, X., Zhao, K., Zhou, Y., Clinton, N., DeVries, B., Golden, H.E., Lang, M.W., 2019. Integrating LiDAR data and multi-temporal aerial imagery to map wetland inundation dynamics using Google Earth Engine. *Remote Sens. Environ.* 228, 1–13. <https://doi.org/10.1016/j.rse.2019.04.015>.
- Wu, Z., Wu, J., Liu, J., He, B., Lei, T., Wang, Q., 2013. Increasing terrestrial vegetation activity of ecological restoration program in the Beijing-Tianjin Sand Source Region of China. *Ecol. Eng.* 52, 37–50. <https://doi.org/10.1016/j.ecoleng.2012.12.040>.
- Wulder, M.A., White, J.C., Loveland, T.R., Woodcock, C.E., Belward, A.S., Cohen, W.B., Fosnight, E.A., Shaw, J., Masek, J.G., Roy, D.P., 2016. The global Landsat archive: Status, consolidation, and direction. *Remote Sens. Environ.* 178, 271–283. <https://doi.org/10.1016/j.rse.2015.11.032>.
- Xu, D., You, X., Xia, C., 2019. Assessing the spatial-temporal pattern and evolution of areas sensitive to land desertification in North China. *Ecol. Ind.* 97, 150–158. <https://doi.org/10.1016/j.ecolind.2018.10.005>.

- Xue, Z., Qin, Z., Li, H., Ding, G., Meng, X., 2013. Evaluation of aeolian desertification from 1975 to 2010 and its causes in northwest Shanxi Province, China. *Global Planet. Change* 107, 102–108. <https://doi.org/10.1016/j.gloplacha.2013.05.001>.
- Yu, H., Lee, J.-Y., Lee, W.-K., Lamchin, M., Tserendorj, D., Choi, S., Song, Y., Kang, H.D., 2013. Feasibility of vegetation temperature condition index for monitoring desertification in Bulgan, Mongolia 29 (6), 621–629. <https://doi.org/10.7780/kjrs.2013.29.6.5>.
- Yuan, W., Zheng, Y., Piao, S., Ciais, P., Lombardozzi, D., Wang, Y., Ryu, Y., Chen, G., Dong, W., Hu, Z., Jain, A.K., Jiang, C., Kato, E., Li, S., Lienert, S., Liu, S., Nabel, J.E.M.S., Qin, Z., Quine, T., Sitch, S., Smith, W.K., Wang, F., Wu, C., Xiao, Z., Yang, S., 2019. Increased atmospheric vapor pressure deficit reduces global vegetation growth. *Sci. Adv.* 5, eaax1396. <https://doi.org/10.1126/sciadv.aax1396>.
- Zhang, C., Wang, X., Li, J., Hua, T., 2020. Identifying the effect of climate change on desertification in northern China via trend analysis of potential evapotranspiration and precipitation. *Ecol. Ind.* 112, 106141. <https://doi.org/10.1016/j.ecolind.2020.106141>.
- Zhang, C.-L., Li, Q., Shen, Y.-P., Zhou, N., Wang, X.-S., Li, J., Jia, W.-R., 2018a. Monitoring of aeolian desertification on the Qinghai-Tibet Plateau from the 1970s to 2015 using Landsat images. *Sci. Total Environ.* 619–620, 1648–1659. <https://doi.org/10.1016/j.scitotenv.2017.10.137>.
- Zhang, J., Niu, J., Buyantuev, A., Wu, J., 2014. A multilevel analysis of effects of land use policy on land-cover change and local land use decisions. *J. Arid Environ.* 108, 19–28. <https://doi.org/10.1016/j.jaridenv.2014.04.006>.
- Zhang, R., Xu, X., Liu, M., Zhang, Y., Xu, C., Yi, R., Luo, W., 2018b. Comparing ET-VPD hysteresis in three agroforestry ecosystems in a subtropical humid karst area. *Agric. Water Manag.* 208, 454–464. <https://doi.org/10.1016/j.agwat.2018.06.007>.
- Zhang, Z., Huisingsh, D., 2018. Combating desertification in China: monitoring, control, management and revegetation. *J. Cleaner Prod.* 182, 765–775. <https://doi.org/10.1016/j.jclepro.2018.01.233>.
- Zhou, Y., Dong, J., Xiao, X., Liu, R., Zou, Z., Zhao, G., Ge, Q., 2019. Continuous monitoring of lake dynamics on the Mongolian Plateau using all available Landsat imagery and Google Earth Engine. *Sci. Total Environ.* 689, 366–380. <https://doi.org/10.1016/j.scitotenv.2019.06.341>.
- Zhu, X., Leung, K.H., Li, W.S., Cheung, L.K., 2020. Monitoring interannual dynamics of desertification in Minqin County, China, using dense Landsat time series. *Int. J. Digital Earth* 13 (8), 886–898. <https://doi.org/10.1080/17538947.2019.1585979>.
- Zhu, Z., Woodcock, C.E., 2014. Automated cloud, cloud shadow, and snow detection in multitemporal Landsat data: An algorithm designed specifically for monitoring land cover change. *Remote Sens. Environ.* 152, 217–234. <https://doi.org/10.1016/j.rse.2014.06.012>.
- Zolotokrylin, A.N., Gunin, P.D., Titkova, T.B., Bazha, S.N., Danzhalova, E.V., Kazantseva, T.I., 2016. Diagnosis of the desertification dynamics of arid pastures in Mongolia from observation in key areas and MODIS data. *Arid Ecosyst.* 6 (3), 149–157. <https://doi.org/10.1134/S2079096116030100>.